Ultrastructure of the Proximal Tubule of the Rhesus Monkey Kidney

C. Craig Tisher, MD,* Seymour Rosen, MD,† and George B. Osborne

THE FINE STRUCTURE of the normal nonprimate mammalian kidney has been a favorite subject of investigators.[1-20] With the exception of the human, however,[19,21-28] the primate kidney has received very little attention.[29-33] This investigation was undertaken to define the ultrastructure of the proximal tubule of the nondiseased rhesus monkey (*Macaca mulatta*) kidney and to compare the findings with those noted previously in the nondiseased human kidney. A second goal of the study was the determination of the ultrastructural alterations that can be ascribed to the methods of procurement and preparation of percutaneous renal biopsies. Therefore, in each animal, renal tissue was prepared for electron microscopy by immersion fixation of percutaneous biopsies and by in-vivo intravascular perfusion of the intact kidney using several different fixative and buffer combinations.

Materials and Methods

Eight young healthy rhesus monkeys (*Macaca mulatta*), 6 males and 2 females, weighing 2.7–4.4 kg were studied.‡ The animals were fed a standard laboratory diet supplemented with fresh fruit and were allowed free access to water. They were housed in individual cages and placed periodically in metabolic chairs (Foringer—Rockville, Md) to facilitate collection of urine and blood samples. To determine that the animals were generally healthy and free of renal disease, the following laboratory tests were performed on some or all of the animals: creatinine, sodium, potassium, chloride, total carbon dioxide, plasma urea nitrogen, hematocrit, white blood cell count, urinalyses, and 24-hr creatinine clearances. The results of these tests are tabulated in Table 1.

A percutaneous renal biopsy was performed on each animal and the tissue was immediately placed in fixatives for light and electron microscopy. Later, each animal was opened abdominally and in 5 of the 8 animals, the previously biopsied kidney was removed and fixed for light microscopy. The remaining kidney was

From the Department of Metabolism, Walter Reed Army Institute of Research Washington, D.C. 20012.

Accepted for publication May 28, 1969.

Address for reprint requests: C. Craig Tisher, Department of Medicine, Duke University Medical Center, Durham, NC 27706.

* Present Address: Department of Medicine, Duke University Medical Center, Durham, NC 27706.

† Present Address: Department of Pathology, Beth Israel Hospital, Boston, Mass.

‡ In conducting the research described in this report, the investigators adhered to the *'Guide for Laboratory Animal Facilities Care,'* as promulgated by the Committee on the Guide for Laboratory Animal Facilities and Care of the Institute of Laboratory Animal Resources, National Academy of Sciences—National Research Council.

Table 1. Results of Laboratory Tests

Test	Animal							
	I	II	III	IV	V	VI	VII	VIII
Plasma urea nitrogen (mg/100 ml)	16.6	11.5	17.2	15.7	17.4	13.7	17.4	25.5
Creatinine (mg/100 ml)	0.77	0.71	0.75	0.67	0.98	0.98	0.74	0.67
Sodium (mEq/liter)	148	149	149	—	141	152	150	152
Potassium (mEq/liter)	4.9	4.6	5.2	—	3.0	5.0	4.6	3.7
Chloride (mEq/liter)	—	111	107	—	104	107	105	104
Total carbon dioxide (mEq/liter)	—	21.7	21.1	—	27.0	21.2	23.0	29.0
Hematocrit (Volumes %)	—	39	37	40	38	39	40	37
WBC count (cu mm)	—	11,300	7650	4900	7400	12,900	6800	10,500
Urine albumin	—	Neg	Neg	Neg	Neg	Neg	Neg	Neg
Urine sediment	—	—	—	Neg	Neg	—	Neg	Neg
Creatinine clearance (ml/min/kg)	—	3.2	2.5	3.2	—	2.2	3.2	3.5

perfused intravascularly with glutaraldehyde or osmium tetroxide in a manner similar to that described by Griffith, Bulger, and Trump.[20] In 3 of the 8 animals, the biopsied kidney was not removed and both were perfused. In all biopsy and surgical procedures, Sernylan (Parke, Davis and Company) or Sernylan supplemented with pentobarbital was used as the anesthetic agent. In the in-vivo intravascular perfusion procedure, the kidneys were usually "flushed" with 15–25 ml of isotonic saline and then immediately perfused with fixative at 25°–37° for 1–5 min at a constant pressure of 160–180 mm Hg. After immediate excision, the kidney was divided into specific regions, including the outer cortex, juxta-medullary cortex, outer medulla, and inner medulla, and processed for electron microscopy. In addition, sagittal sections, 1–2 mm thick, extending from the cortex to the papillary tip, were taken in some animals.

Preparation for Electron Microscopy

Tissues obtained by percutaneous biopsy were immediately diced into 1 mm cubes and placed in a variety of fixatives. Tissue preserved by in-vivo intravascular perfusion was handled in a similar manner. The fixatives employed were (A) 1% osmium tetroxide in phosphate buffer—total duration of fixation, 1–1½ hr; (B) 2% osmium tetroxide in 0.1 M *s*-collidine—total duration of fixation, 1–2 hr; (C) 2% glutaraldehyde in 0.025–0.1 M sodium cacodylate buffer—total duration of fixation, 5–6 hr—rinsed in 0.067–0.1 M sodium cacodylate buffer with 5% sucrose for 16 hr and post-fixed in 2% osmium tetroxide in 0.1 m *s*-collidine or 1% osmium tetroxide in phosphate buffer for 1 hr; (D) 6.25% glutaraldehyde buffered in 0.1 M sodium cacodylate—total duration of fixation, 6 hr—rinsed in 0.1 M sodium cacodylate with 7.5% sucrose for 16 hr, and post-fixed 1 hr in 2% osmium tetroxide in 0.1 M *s*-collidine; (E) Same as (D) except post-fixation in 1% osmium tetroxide in phosphate buffer for 1 hr. The fixatives used in each animal are listed in Table 2.

All tissue underwent dehydration in a graded series of alcohols and was embedded in Epon epoxy resin.[34] Ultrathin sections were cut on Porter-Blum and LKB ultramicrotomes with glass and diamond knives. Sections were mounted on both supported and unsupported copper grids and were stained in aqueous uranyl

Table 2. Method of Tissue Preservation

Animal	Method	
	Immersion biopsy	IVIP*
I	A	A
II	A,B,D	†
III	B,C	B
IV	B,C	C
V	A,B,C	C
VI	A,B,C	D,E
VII	A,B,C,E	†
VIII	A,B,D,E	A

* In-vivo intravascular perfusion.
† Unsuccessful perfusion.

acetate [25] for 10–120 min and counterstained with lead citrate [26] for 3–10 min before examination in an RCA EMU-3H electron microscope.

Acid Phosphatase Preparation

In 3 animals, acid phosphatase preparations were performed according to the technique of Ericsson and Trump [3] but with the following modifications. The primary fixative was 2% glutaraldehyde buffered with 0.1 M sodium cacodylate; tissue was stored up to 5 days in 0.067–0.1 M sodium cacodylate buffer with 5% sucrose added; frozen sections were cut at 30 μ, and incubation periods varied from 15–20 min; the acetic acid rinse was shortened to 15 sec.

Control material was incubated in Gomori medium without substrate or in a complete medium to which 0.01 M sodium fluoride was added. Uranyl acetate alone was used to stain ultrathin sections of the acid phosphatase preparations.

Preparation for Light Microscopy

Biopsy and excised kidney tissue for light microscopy was fixed in either Zenker-formal or phosphate-buffered 10% formalin. Tissue was dehydrated in alcohols and embedded in paraffin. Sections 3 μ thick were stained with hematoxylin and eosin and the periodic acid-Schiff (PAS) and Gomori's trichrome techniques.[27] In some instances, discrete portions of the kidney were dissected and sectioned serially.

For each animal, 0.5–1.0 μ survey sections of the epoxy-embedded tissues were stained with toluidine blue [28] and examined by light microscopy.

Basement Membrane Measurements

Measurements of the thickness of basement membranes were made on representative pictures of all three segments of the proximal tubule of kidneys fixed by in-vivo intravascular perfusion and of only the first segment of immersion-fixed biopsy tissue obtained from the same animals. Equal numbers of pictures from tissue fixed in osmium tetroxide and glutaraldehyde were chosen. Care was taken to avoid selection of pictures containing tangentially sectioned basement membrane, but otherwise the selection was completely randomized and included material from 7 of the 8 animals. A total of 448 measurements were made on 112 photographs. On each picture, four measurements were made which included the thickest and thinnest areas of the basement membrane. The magnification of the electron microscope was determined using a carbon replica of an optical grating with 28,800 lines/in. All data was analyzed statistically using the non-paired T test. All results are tabulated in Table 3 and 4.

Table 3. Comparison of Basement Membrane Thickness in Three Segments of the Proximal Tubule of the Rhesus Monkey

Segment	No. of measurements	Minimum thickness		Maximum thickness	
		Mean ± SEM (Å)	Range (Å)	Mean ± SEM (Å)	Range (Å)
First	56	2550* ± 107	1257–4470	3845* ± 154	2184–6515
Second	56	1460* ± 83	680–3333	2672* ± 137	1162–5833
Third	56	703 ± 28	363–1101	1523 ± 67	731–3252

* p = <0.001 compared with third segment.

Results

Light Microscopy—In-Vivo Intravascular Perfusion (IVIP)

Three distinct segments of the proximal tubule were identified by both light and electron microscopy. These segments were defined by the morphology of their individual cellular components and by their relationship to other regions of the nephron. The first segment which, in general, corresponded to the *pars convoluta* began as an abrupt transition from the flattened squamous epithelial cells lining Bowman's capsule to tall columnar cells which exhibited a well developed PAS positive brush border (Fig 1). This transition was observed by light microscopy on numerous occasions in each animal and studied by electron microscopy a total of five times in five different animals; its appearance was always the same. In optimally preserved material fixed by IVIP, open tubular lumens were seen in all three segments of the proximal tubule. By light microscopy, the columnar cells of the first segment were slightly taller than those of the second segment and possessed a longer and more regularly structured brush border (Fig 2). The mitochondria were closely packed and generally elongate. The cells of the first segment stained more intensely with toluidine blue than those in the other two segments of the proximal tubule.

Cells composing the middle or second segment of the proximal tubule were low columnar in shape and possessed a shorter and often more irregular brush border than the first segment (Fig 3). Mitochondria were more tortuous and seldom elongate. The accumulation of lipid droplets near the cell base was a more constant feature within this region and helped distinguish it from the first segment.

By identifying the beginning of the descending portion of the proximal tubule on large sagittal sections it was possible to define a gradual transition from the middle or second segment to the third segment, the latter corresponding in general to the distal *pars recta*. The cells of the third segment were cuboidal in shape, exhibited a convex luminal surface

covered by a distinct brush border, and contained fewer organelles than the first two segments of the proximal tubule (Fig 4). There was a gradual transition from the terminal proximal tubule to the thin descending limb of Henle (Fig 5). The cells comprising the terminal proximal tubule and early thin limb generally contained large accumulations of lipofuscin, which on hematoxyln and eosin sections appeared golden brown in color.

Electron Microscopy—In-Vivo Intravascular Perfusion (IVIP)

In confirmation of the light microscopy findings, the transition from the low-lying parietal epithelium lining Bowman's capsule to the tall columnar epithelial cells of the initial portion of the first segment of the proximal tubule was abrupt (Fig 6).

First Segment

In the first segment of the proximal tubule, interdigitations of the tall columnar cells with one another were extensive, particularly at the cell base (Fig 7 and 8). However, true basilar infoldings where the infolded plasma membrane returned to the original point of inflection were not observed. In both the first and second segments of the proximal tubule, evaginations of the base of the cell projecting into folds or outpouchings of the basement membrane were frequently observed (Fig 9). Bands of coarse fibrils extended perpendicularly across the mouth's or neck's of most of these cellular evaginations.

The junctional complexes resembled those of the human kidney. The *zonula occludens*, or tight junction, nearest the tubular lumen, was very narrow, while the *zonula adhaerens*, or intermediate junction, situated immediately beneath the *zonula occludens*, was much wider. The *macula adhaerens*, or desmosome, was situated between the intermediate junction and the cell base.

Apical Cell Region. The plasma membrane along the apical cell boundary formed a brush border composed of long slender microvilli. Between the microvilli, deep invaginations of the plasma membrane formed open tubular structures which appeared on cross section as small coated vesicles (Fig 10 and 11). The small coated vesicles exhibited an organized internal lining of short filaments resembling the glycocalyx of the apical cell membrane. Externally, these same vesicles had a coating of radially directed short bristles or spines identical to the bristle-like or spiney layer on the intracellular side of the deep invaginations of the apical plasmalemma.

A second distinct type of coated vesicle was also evident, especially

Table 4. Comparison of Basement Membrane Thickness of the First Segment of the Proximal Tubule Fixed in Glutaraldehyde and Osmium Tetroxide

Fixative	Method of fixative application	No. of measurements	Minimum thickness		Maximum thickness	
			Mean ± SEM (Å)	Range (Å)	Mean ± SEM (Å)	Range (Å)
Glutaraldehyde	Immersion	28	2569 ±168	1302–4039	4280 ±263	2344–7374
Osmium tetroxide	Immersion	28	3578* ±315	1644–7308	5692† ±340	2898–9799
Glutaraldehyde	IVIP‡	30	2518 ±154	1257–4258	4013 ±180	2204–6194
Osmium tetroxide	IVIP‡	26	2588 ±153	1502–4470	3650 ±261	2184–6515

* $p = <0.01$.
† $p = <0.001$.
‡ In-vivo intravascular perfusion.

in tissue preserved by IVIP with 6.25% glutaraldehyde. These vesicles were larger and possessed a dense internal lining and, in many instances, a definite internal limiting membrane (Fig 10 and 11). In the majority of these structures there was no bristle-like layer external to the outer limiting membrane as noted with the first type of apical vesicle.

Large apical vacuoles were common in this segment (Fig 7). These vacuoles possessed an internal flocculent lining similar to the smaller apical vesicles but were devoid of an external bristle coat.

In addition to the tubular structure formed as a result of grazing or tangential sectioning of the invaginations of the apical plasmalemma, an extensive system of dense tubules was observed coursing through the apical region of the cell. They were commonly observed in direct connection with the larger type of apical vesicles described above (Fig 10 and 11). Cross-sections of this tubular system gave rise to a third type of small dense circular structure (Fig 11). Dense tubules were occasionally observed opening directly into lateral intercellular spaces in the apical cell region (Fig 12).

Mitochondria. The mitochondria were generally elongated and rather tortuous structures which frequently extended from the cell base to the cell apex (Fig 7). Within this segment of the proximal tubule they were often closely associated with plications of the basal plasmalemma (Fig 7 and 8). The cristae were generally oriented at right angles to the axis of the mitochondrion. Matrical granules were electron dense and often had a rosette configuration. The presence of intramitochondrial inclusions was an interesting finding. These will be described in more detail in a later section of this paper.

Golgi complex, endoplasmic reticulum, and ribosomes. Within the first segment of the proximal tubule, the Golgi complex was located in the upper half of the cell lateral to or above the nucleus and was composed of cisternae and various sized vesicles (Fig 7). Profiles of smooth- and rough-surfaced endoplasmic reticulum were present in abundant quantities throughout the cells of the first segment. The largest aggregations of endoplasmic reticulum were arranged in "stacks" contiguous with clusters of elongate microbodies (Fig 13). Free ribonucleonprotein particles (RNP) were scattered throughout the cells, but were present in greatest concentration in the lower two-thirds of the cell.

Microbodies. Microbodies were the most common single membrane-limited inclusion body (SMLIB) observed in the first segment of the proximal tubule. In optimally preserved tissue fixed by IVIP with glutaraldehyde or osmium tetroxide, most microbodies were dense elongate structures measuring up to 1.2 μ in length and 0.8 μ or greater in width.

They were always closely associated with profiles of smooth- and rough-surfaced endoplasmic reticulum. When observed in clusters, the long axis of the microbody was oriented parallel to cisternal profiles or "stacks" of smooth- and rough-surfaced endoplasmic reticulum (Fig 13–15). The microbody possessed one or two peripheral linear densities or marginal plates [39] which were contiguous with the inner aspect of the outer limiting membrane of the organelle. The endoplasmic reticulum was usually closely associated with that portion of the outer limiting membrane adjacent to the marginal plate of the microbody. Regardless of the fixative employed, when tissue was preserved by IVIP, the microbody matrix was more dense than the surrounding cytoplasm and was usually more dense than the matrix of adjacent mitochondria. In optimally preserved tissue, dense nucleoid structures were not observed within the microbody.

The marginal plate was often multilayered, each layer measuring approximately 150 Å in thickness (Fig 14). The individual layers exhibited a regular periodicity of 125 Å, suggesting the existence of a well-organized internal structure (Fig 14 and 15).

Cytosomes. In the early "neck" region, cytosomes containing multiple small dense inclusions were present, generally in the apical region of the cell (Fig 16). Rarely were similar appearing cytosomes observed in more distant regions of the proximal tubule. Throughout the remainder of the first segment, cytosomes were numerous and often very irregular in shape. In tissue preserved by IVIP with 1% osmium tetroxide in phosphate buffers, the majority of the cytosomes were very electron dense, exhibited a homogeneous background matrix, and often contained membranous fragments and other debris (Fig 17). In marked contrast, the majority of cytosomes in similar tissue preserved by IVIP with 2% osmium tetroxide buffered with *s*-collidine demonstrated an extremely pale, homogeneous background matrix (Fig 18). Again, many of the bodies contained membranous fragments and other debris. The majority of cytosomes observed in tissue preserved by IVIP with 6.25% glutaraldehyde were dense and homogeneous in character (Fig 19). Regardless of the fixative employed, frequent "intermediate" morphologic forms of cytosomes were present throughout the cells of the first segment of the proximal tubule.

Cytosegresomes (*autophagic vacuoles*). This type of cytoplasmic body, which contains recognizable organelles surrounded by one or more outer limiting membranes, was much less common throughout the initial or first segment of the proximal tubule than were the cytosomes. Cytosegresomes were distributed randomly through the proximal tubule cells. The most frequent cellular organelle within the cytosegresome was

the mitochondrion, although microbodies, multivesicular bodies, and free RNP particles (ribosomes) were also observed (Fig 19–21).

Multivesicular Bodies. Within the first segment, multivesicular bodies were the least common SMLIB of the four types present. When observed, they were usually located in the apical region of the cell or near the Golgi complex. They varied considerably in size and appearance. The background matrix was characteristically pale and the vesicular components were usually uniform in size (Fig 7). Vesicles of similar appearance were sometimes located adjacent to these bodies. Some multivesicular bodies exhibited a dense background matrix while others contained vesicles of several sizes. The latter type of inclusion body was not observed near the Golgi complex.

Lipid. In the first segment, lipid droplets which appeared to be membrane-bound were present in small numbers near the cell base (Fig 8 and 9). In glutaraldehyde-fixed tissue, most lipid droplets appeared electron lucent, but occasionally they contained small collections of irregular membranous fragments. In osmium tetroxide-fixed tissues, the lipid droplets were homogeneous and slightly more radiopaque in appearance; however, the presence of a limiting membrane was less obvious.

Basement Membrane. The basement membrane of the first segment of the proximal tubule was continuous with that of Bowman's capsule and its appearance was identical. It was composed of a homogeneous dense ground substance containing numerous fine filaments. It was occasionally multilayered or laminated and extremely variable in thickness, ranging from 1257 to 6515 Å, in tissue fixed by IVIP. The mean values of the thinnest and thickest regions of the basement membrane made on 28 representative electron micrographs were 2550 ± 107 Å and 3845 ± 154 Å, respectively (Table 3). As shown in Table 4, there was no significant difference in membrane thickness between the tissue fixed in osmium tetroxide and that fixed in glutaraldehyde, when the fixatives were applied by IVIP. Frequently, bundles of filaments were observed at the base of proximal tubule cells adjacent to the basement membrane (Fig 9).

Nucleus. The nucleus within the cells of this segment of the proximal tubule were basally-placed and generally spherical in shape. They resembled the nuclei described in other mammalian proximal tubules.

Ground Substance. The ground substance of cells in the first segment of the proximal tubule was composed of a uniform thin flocculent material. In glutaraldehyde-fixed tissue, the ground substance was more dense than that of tissue preserved primarily in osmium tetroxide. In

addition to the organelles and structures described in the preceeding paragraphs, an extensive system of microtubules was present coursing throughout the cell. This system was most evident in glutaraldehyde-fixed tissue.

Second Segment

Cells comprising the second segment of the proximal tubule were generally simpler in shape and configuration, and basilar invaginations of the plasmalemma enclosing mitochondrial profiles were less common. Again, true basilar infoldings of the plasmalemma were not observed. The junctional complexes were similar to those in the first segment.

The microvilli forming the brush border were shorter, more irregular, and more widely separated when contrasted to those in the first segment, and invaginations of the apical plasmalemma were usually shallower (Fig 22). The apical vesicles and tubules were similar in appearance but not as extensively developed as in the first segment. However, large apical vacuoles were more prevalent in this region, a feature which was discernible by both light and electron microscopy.

Elongate mitochondria were less frequent in the second segment, the majority being more spherical or ovoid. The internal configuration was identical to its counterpart in the first segment.

The Golgi complex did not vary in configuration or position from its counterpart in the first segment and the concentration of the smooth- and rough-surfaced endoplasmic reticulum as well as the free ribosomes was similar to the first segment. There was no marked difference in the configuration, number, or distribution of cytosomes, cytosegresomes, microbodies, or multivesicular bodies in the second segment when compared with the first segment. However, lipid droplets were more common in the second segment than the first. Although similar in appearance, the basement membrane was considerably less thick in the second segment than the first. The mean values of the thinnest and thickest regions of the membrane were 1460 ± 83 Å and 2672 ± 137 Å, respectively. The membrane varied in thickness from 680 to 5833 Å (Table 3).

Third Segment

Cells of the third segment developed an apical convexity, decreased in height, and assumed a cuboidal configuration (Fig 23). Basal plasmalemma invaginations and lateral cell interdigitations decreased markedly and mitochondria were rarely enclosed within plications of the basal plasmalemma.

The apical plasmalemma formed a distinct, but less extensive, brush

border composed of shorter microvilli. In the distal or terminal regions of the third segment, the microvilli were often absent over short segments of the cell surface (Fig 24).

Deep invaginations of the apical plasmalemma were rarely observed in this segment. Open and dense tubules and large apical vacuoles, although present, were uncommon. However, apical vesicles, particularly the coated variety, were numerous (Fig 23 and 24).

Elongate mitochondria were seldom observed within the third segment of the proximal tubule, but spherical and ovoid forms were numerous. Their internal configuration of cristae and matrical granules resembled other regions of the proximal tubule.

The Golgi complex was well developed and was usually positioned above or lateral to the nucleus. Rough-surfaced endoplasmic reticulum and free ribosomes were not as extensive in this segment, but smooth-surfaced endoplasmic reticulum was abundant.

Microbodies were the most common SMLIB observed in this segment of the proximal tubule (Fig 23). In contrast to the first segment, they seldom displayed an elongate configuration, but were always closely associated with profiles of smooth-surfaced endoplasmic reticulum. Not infrequently, processes extended from these organelles into the surrounding cytoplasm, which probably represented connections with the endoplasmic reticulum (Fig 25).

Multivesicular bodies were more numerous within this segment than in any other region of the proximal tubule. They were scattered throughout the cell but were present in greatest numbers in the apical region, just beneath the microvilli (Fig 24). They varied markedly in size and shape, especially those in the apical cell region. As noted in other segments of the proximal tubule, the vesicles within the bodies varied in number and size. The background matrix within the multivesicular bodies was often very dense.

Cytosomes and especially cytosegresomes were relatively uncommon throughout most of the third segment of the proximal tubule. When present, most cytosomes were homogeneous in character, their density depending primarily on the type of fixative employed. In the terminal portions of this segment at the transition into the thin descending limb of Henle, large collections of lipofuscin were frequently observed (Fig 26). Lipid droplets were not common in this segment of the proximal tubule.

The appearance of the cell nucleus and ground substance was identical to that in other regions of the proximal tubule.

The basement membrane was similar in appearance to that in other

segments of the proximal tubule. However, its thickness was significantly less, varying from 363 to 3252 Å. The mean values of the thinnest and thickest areas of the membrane were 704 ± 28 Å and 1523 ± 67 Å, respectively (Table 3).

Transition into thin limb of Henle. The transition from the third or terminal segment of the proximal tubule to the early descending thin limb of Henle's loop was gradual (Fig 5 and 27). Often, as observed by light microscopy, cells characteristic of the thin limb were interspersed with those of the proximal tubule for short distances.

Light Microscopy—Immersion-fixed Biopsy Tissue

It was not always possible to clearly define the three segments of the proximal tubule in the tissue obtained by percutaneous renal biopsy. This problem was due to both sampling deficiencies, resulting in failure to obtain regions containing the third and terminal segments of the proximal tubule, and inadequate tissue preservation, making identification of the individual segments extremely difficult.

Most of the proximal tubules were not patent (Fig 28). This appeared to be due to cell swelling, resulting in cellular debris filling the lumen, rather than to tubular collapse *per se*. General cellular organization was disrupted in many tubules and the brush border was often indistinct. Apical vacuoles and elongate mitochondrial profiles, which are usually visible at the light microscopic level on 1μ epon sections, were rarely observed. Greatly widened extracellular spaces were especially prominent. It was interesting to note that in areas of the kidney that were unsuccessfully preserved by IVIP, an identical picture was the result. Figure 29 represents a proximal tubule from such an area.

Electron Microscopy—Immersion-fixed Biopsy Tissue

Observations at the light microscopic level were confirmed and extended by electron microscopy (Fig 30). The occluded proximal tubular lumens contained cellular debris. Cellular swelling, which often affected the entire cell but was more apparent apically, often resulted in interruption of the apical plasmalemma and disruption of the brush border. In such instances, there was general rearrangement of the cellular organelles, many of which appeared to have streamed out of the damaged cells into the tubular lumen (Fig 30). The lateral extracellular spaces were often greatly widened, especially toward the base of the cells. This feature was most evident in tissue fixed with 6.25% glutaraldehyde. Junctional complexes were similar to those in tissue preserved by IVIP.

Apical Cell Region. As noted above, this region of the cell often

underwent extensive alterations in the immersion-fixed tissue. The several components, including apical vesicles, apical vacuoles, and tubules, were not significantly altered individually, but their spatial relationships to one another and to the microvilli were often severely affected (Fig 30).

Mitochondria. In biopsy tissue, mitochondria appeared to be more tortuous, and elongate profiles were much less common (Fig 30). Mitochondrial inclusions were a frequent finding in immersion-fixed tissue obtained by biopsy, but were also evident in the tissue preserved by IVIP. Two morphologic types of intramitochondrial inclusions were observed. The first type of mitochondrial inclusion, composed of helical structures, lay entirely within widened cristae and was not as electron dense as the surrounding matrix (Fig 31). The inclusions were composed of filaments 30–40 Å in width. The diameter of the helix was 130–140 Å with a pitch of approximately 120 Å. The filaments usually ran parallel to one another and often appeared to twist or coil on each other. This was the most common type of mitochondrial inclusion observed in this material.

The second type of inclusion appeared to lie free within the mitochondrial matrix and may have represented a modification of the mitochondrial cristae (Fig 32). It was composed of several parallel rows of membranes which resembled cristae. In some areas along these membranous profiles, a periodicity of 290 Å was present. This apparent periodicity appeared to be the result of twisting of the two parallel membranes to form a double helix (insert, Fig 32). These membranous structures were separated by a 100 Å space which was continuous with the mitochondrial matrix. Short filaments with a spacing of 90 Å bridged this latter space at right angles to the long membranous profiles. A diagram of this structure is shown in Figure 33. All components of this type of inclusion were more electron dense than the surrounding mitochondrial matrix.

Golgi complex, endoplasmic reticulum, and ribosomes. In biopsy tissue fixed by immersion, the Golgi complex usually maintained its position in relation to the cell nucleus similar to that noted in the perfusion-fixed tissue. However, there was a greater tendency for the cisternae to become more widely dilated, often assuming the configuration of large vacuoles rather than the normal flattened and slightly curved sacs (Fig 30). This difference was most obvious in the tissue fixed with 6.25% glutaraldehyde. In general, the poorer the tissue preservation, the more distended and swollen were the cisternal compartments of the Golgi complex.

Similar findings were noted in the appearance of the smooth- and

rough-surfaced endoplasmic reticulum. Again, there was much more swelling and dilatation of the endoplasmic reticulum in the cells fixed by immersion than in those preserved by IVIP. In general, the poorer the overall cellular preservation, the more swollen and distorted the endoplasmic reticulum appeared.

Single membrane-limited inclusion bodies. Of the four main types of SMLIBs described earlier, the microbody appeared to be most significantly altered by the method of fixative application employed. As shown earlier in the tissue optimally preserved by IVIP (Fig 13–15), the microbody was generally an elongate structure exhibiting one or two peripheral linear densities (marginal plates) and a homogenous matrix more dense than the surrounding cytoplasm of the cell. In the immersion-fixed biopsy material and in tissue from areas of the kidney not well fixed by IVIP, the typical microbody assumed varied configurations but still maintained its intimate association with profiles of smooth- and rough-surfaced endoplasmic reticulum. It appeared that considerable swelling had occurred within individual microbodies as evidenced by an apparent overall increase in volume and a definite decrease in matrical density, regardless of the fixative employed. With less severe swelling, the organelles were still elongate, but one or both marginal plates were curved or bent and the adjacent endoplasmic reticulum was widely dilated (Fig 34). With more severe swelling, many microbodies become angulated in configuration as a result of the fracture of one or more of the marginal plates along the outer limiting membrane (Fig 35 and 36). These progressive alterations in the individual organelles coupled with tangential sectioning accounted for the vast majority of the bizzare configurations of the microbodies observed in immersion-fixed tissue. Although these findings were more dependent on the method of fixative application than the type of fixative employed, it was noted that angular configurations of the microbodies were more commonly observed in tissue fixed in 6.25% glutaraldehyde.

Nucleoids, the majority of which were structured, were observed within microbodies in both immersion-fixed tissue and in tissue taken from areas of kidney not well preserved by IVIP. Similar structures were not observed in optimally-preserved tissue fixed by IVIP. A more detailed description of renal microbody nucleoids and their enzymatic composition has recently been reported from this laboratory.[29]

Basement Membrane. The overall appearance of the basement membrane of the proximal tubule in immersion-fixed tissue was similar to that in tissue preserved by IVIP. However, there was a statistically significant difference in the thickness of the basement membrane which was de-

pendent on the type of fixative employed. When analyzed separately, basement membranes of proximal tubules characteristic of the first segment in tissue immersed in osmium tetroxide ranged from 1644 to 9799 Å. The mean values of the thinnest and thickest areas were 3578 ± 315 Å and 5692 ± 340 Å, respectively. In contrast, the mean values of the thinnest and thickest regions of the basement membrane of proximal tubules fixed by immersion in glutaraldehyde were 2569 ± 168 Å and 4280 ± 263 Å, respectively. As shown in Table 4, basement membrane thickness was nearly identical if proximal tubules were perfusion-fixed with osmium tetroxide or glutaraldehyde.

Acid Phosphatase Reaction. Within the proximal tubule cells positive staining (lead precipitate) for the presence of acid phosphatase was noted within cytosomes and Golgi cisternae (Fig 37–39). Reaction product was not observed in other components of the Golgi complex or in the endoplasmic reticulum. The overwhelming majority of cytosomes contained reaction product which was most often distributed diffusely throughout the organelle. However, two other patterns of staining were observed. In some instances there was a distinct tendency toward a heavier peripheral distribution within the cytosome. Not infrequently, circular and rectangular areas within certain cytosomes were completely free of reaction product (Fig 37 and 39). Those cytosomes which did not stain positively for acid phosphatase could not be identified morphologically as a separate group or type. It was not possible to distinguish between cells of the first or second segments of the proximal tubule on the basis of the staining pattern of the cytosomes in this material. The limited number of observations in cells of the third segment precluded precise descriptions of the reaction pattern for acid phosphatase in this region of the proximal tubule.

Discussion

In a study of this type there is always the question of whether the observed morphology truly represents the normal state. Therefore it is important to rule out obvious renal disease in the animal under investigation and to determine the functional state of the kidney at the precise moment of fixation. All of the clinical laboratory tests performed on each animal to rule out obvious renal disease were found to be within the normal limits as established by several previous investigators.[40–47] In all likelihood, the animals were antidiuretic at the time of the percutaneous renal biopsies and later when perfused intravascularly. Griffith, Bulger, and Trump,[20] working with rats and employing similar surgical and perfusion techniques, observed elevated osmolar U/P ratios

after the surgical trauma connected with cannula implantation preceding the actual intravascular perfusion.

Present evidence indicates that the technique of in-vivo intravascular perfusion results in tissue preservation that closely represents the in-vivo functioning state of the organ.[20] Therefore, comparison of tissue preserved by in-vivo intravascular perfusion-fixation with tissue obtained by biopsy from the same animal and preserved by immersion-fixation in identical fixative and buffer combinations affords the opportunity to define more clearly preparation artifacts at both the light and electron microscopic level. In-vivo intravascular perfusion-fixation is obviously not a technique applicable to human renal tissue. Since, however the fine structure of the proximal tubule in the rhesus monkey was similar in most respects to that of man, most of the findings regarding preparation artifact and tissue distortion can be directly related to human renal biopsies. Several different fixatives were employed in this study; however no attempt will be made to systematically compare their varying effects on cell structure since several earlier investigations have defined these parameters of fixation quite well.[11,17]

In general, the differences in results obtained by the two methods of tissue preservation could be classified into two categories—those affecting the entire cell and those affecting individual cellular organelles. Proximal tubules of immersion-fixed tissue exhibited occluded lumens containing cellular debris and the apical portions of swollen epithelial cells. The apical plasmalemma was often disrupted and the microvilli comprising the brush border were greatly distorted. Lateral intercellular spaces were distended. Rearrangement of cellular organelles was commonplace. Similar findings were noted in kidney areas not successfully fixed by in-vivo intravascular perfusion. Since the fixatives, buffers, and subsequent tissue processing were identical in all respects for the two methods of tissue preservation employed, the observed differences in results must be ascribed to the method of fixative application. In all likelihood these changes are directly related to interruption of the blood supply to the tissue before adequate fixation has taken place. Evidence for this conclusion has been provided in the rat kidney.[20] Intentional interruption of the blood supply, before in-vivo intravascular perfusion-fixation was initiated, resulted in tissue preservation similar to that observed with immersion-fixation in our study. The exact physiologic mechanism that accounts for these observed changes is not completely understood. However, the alterations occur very rapidly, probably within a matter of seconds as noted by Longley and Burstone [48] and Griffith, Bulger, and Trump.[20] Taking these observations into consideration it

appears likely that with cessation of blood flow through the peritubular capillaries surrounding the proximal tubules, the cells are no longer able to effectively transport sodium at their lateral and basilar cell margins. Passive movement of sodium followed by water continues at the apical surface. Rapid cellular swelling results in and leads to disruption of the apical plasmalemma, rearrangement of cellular structure, and damage to cellular organelles. It is possible that changes in the intraluminal hydrostatic pressure also contribute to these cellular alterations.

Differences in the appearance of individual cellular organelles were quite obvious with the two methods of fixative application. Mitochondria were much more tortuous and swollen with fewer elongate profiles being present in the biopsy material. Trump and Bulger,[49-51] studying the isolated flounder tubule, showed that mitochondria typically respond to cell injury by becoming initially more tortuous and swollen and later spherical in shape. Because of the rapidity of these changes it appears most likely that the mitochondrial alterations, as well as similar changes in other cellular organelles, reflect their sudden exposure to increased intracellular concentrations of sodium and water as discussed above. Other cellular alterations which were observed in the immersion-fixed tissue, including dilatation of the endoplasmic reticulum and dilatation of the Golgi cisternae, are equally ascribable to the same mechanism.

The microbody undoubtedly responded in the most dramatic fashion to its sudden exposure to an abnormal intracellular environment. In the perfusion-fixed tissue, microbodies were elongate, electron dense organelles displaying one or two linear densities or marginal plates along their outer limiting membrane. However, in biopsy tissue obtained from the same animals and exposed to the same fixative and buffer solutions but fixed by immersion, the microbodies were swollen as evidenced by an increased volume, a decreased matrical density, bending, angulation, and, in some cases, actual fracture of the marginal plates. In tissue taken from kidney areas not well preserved by in-vivo intravascular perfusion, identical alterations in the microbodies were observed. A more detailed description of these findings can be found in an earlier study.[29]

It is especially important to recognize the cellular alterations which depend on the method of tissue preservation employed since they are identical in many respects to fine structural changes occurring in response to specific forms of cellular injury. In fact, there may well be a common pathway primarily dependent on shifts of extracellular fluid into the cell that leads to many of these morphologic alterations. In the in-vitro isolated flounder tubule model, mechanical damage [49] or exposure to cyanide [50,51] or media of high potassium concentration [52] results

in general cell swelling, dilatation and degranulation of endoplasmic reticulum, and mitochondrial alterations such as matrical swelling. In the case of cyanide injury, the structural alterations correlate well with the presence of increased intracellular concentrations of sodium, chloride, and water.[50] The cellular response to injury in the above experiments requires minutes to hours, while the changes in our study occurred in only a few seconds. However, this probably reflects the magnitude of the insult, namely the complete and irreversible cessation of the blood supply, rather than a significant difference in the mechanism of the response by the individual cells. As noted previously in the rat kidney,[20] the initial phases of cell swelling related to cessation of blood supply were not only rapid but were also very marked, thus paralleling the findings in this study.

The morphology of the proximal tubule in the rhesus monkey kidney was very similar to that of the human. The presence of three distinct segments has not previously been described in the proximal tubule of a primate kidney,[23,27,28] although this segmentation is well known in nonprimate vertebrate kidneys.[9,53,54] The failure to observe this segmentation in earlier primate studies, particularly in man, is probably related to the type of tissue that was available for study and to the method of tissue preservation rather than representive of a true morphologic difference. Even in the present study, positive identification of the various segments of the proximal tubules in the immersion-fixed biopsy tissue was not always possible, even though no difficulty in identification was encountered in perfusion-fixed tissue from the same animals. The general cell shape, size, and configuration of the proximal tubule cells were nearly identical in man and rhesus monkey. One notable difference, however, was the presence of occasional distinct outpouchings or evaginations at the base of a proximal tubule cell of the monkey (Fig 9). These structures were observed in the first two segments of the tubule. Bands of coarse fibrils extended across the mouths or necks of most of these evaginations. The appearance of the cytoplasm within the evaginations was not unlike that of the remainder of the cell nor was the basement membrane any different in its structure at these points. The functional significance of these structures, if any, was not obvious. Although similar appearing bands of fibrils were noted near the basement membranes of nondiseased human proximal tubule cells,[23] outpouchings were never observed.

Cytosomes varied in their morphology and relative number in monkey and man. In the *pars convoluta* of the human proximal tubule, cytosomes containing multiple small dense inclusions presumably representing re-

absorbed constituents of the tubular fluid such as protein were numerous.[23] In the monkey, similar appearing cytosomes were observed in very limited numbers, chiefly in the early neck region of the proximal tubule. Other morphologic types of cytosomes were similar in distribution throughout the remainder of the proximal tubule in the two species. Cytosomes were the most common SMLIB present within the proximal tubule of the human kidney, whereas the microbody was the most common throughout the rhesus monkey proximal tubule. Since the precise function of the microbody in either animal is unknown, the significance of the large number in the monkey is unclear. Uricase is not present in the renal microbodies of either animal.[29,55]

The structure of the microbody in the monkey was considerably different than that of man. In the perfusion-fixed tissue, the microbodies of the monkey were dense, elongate organelles and exhibited one or more marginal plates. The marginal plates were often multilayered as shown in Figure 14. With immersion-fixation the microbodies appeared to swell and the marginal plates became distorted and often fractured giving rise to bizzare angulated structures. Structured nucleoids were often encountered in the microbodies of immersion-fixed tissue after swelling and matrical rarefaction.[29] Similar structures were not observed in optimally preserved perfusion-fixed tissue. In the human biopsy tissue, angulated forms were virtually nonexistent and elongate profiles were not observed.[23,28] Nucleoids were present in an occasional human microbody but did not appear structured.

In the human kidney, lipid inclusions have been observed to be present in greatest numbers within the *pars recta* of the proximal tubule,[23] which is similar to that of the dog.[56] In the rhesus monkey, lipid droplets were present in small numbers in the first and third segments but were most prominent in the second segment of the proximal tubule.

The presence of two types of intramitochondrial inclusions within the proximal tubule cells was an interesting morphologic finding, although the functional or physiologic significance of these structures is not readily apparent. The first type of inclusion observed appears to be nearly identical in configuration to those described by Mugnaini [57] in astrocytic mitochondria of the rat corpus striatum and the dimensions of the inclusions were almost identical. Iseri *et al* [58] and Porta *et al* [59] reported the same type of inclusions in liver mitochondria following alcohol ingestion. Svoboda and Higginson [60] described similar appearing inclusions in the hepatic cells of rats fed protein deficient diets. As pointed out by Mugnaini [57] it is possible that such intramitochondrial inclusions could be the result of fixation and, hence, artifactual. However, we believe this

to be unlikely in our material since these inclusions were observed with both glutaraldehyde and osmium tetroxide fixatives, in the presence of different buffers, and in perfusion-fixed tissues as well as immersion-fixed tissue. Whatever the exact chemical nature of these intramitochondrial inclusions, whether phospholipids, as surmised by Svoboda and Higginson,[60] or macromolecules of protein native, as suggested by Mugnaini,[57] it is apparent that they can exist in normal as well as abnormal functional states. Moreover, they are not confined to a single organ, nor are they found only in rats. Neither type of mitochondrial inclusion observed in the present study has been reported previously in the kidney, although Suzuki and Mostofi [61] have reported other types of inclusions termed "intramitochondrial filamentous bodies (IMFB)" in the ascending thick limb of Henle of the rat kidney. In rats with glycerin-induced acute tubular necrosis and in normal control animals, three types of mitochondrial inclusions were observed by the latter authors, but tubular segments of the nephron other than the thick ascending limb did not contain such structures. Mitochondrial inclusions have not been reported in nondiseased human proximal tubules.[23,27,28]

The present study clearly demonstrated that the thickness of the basement membrane of the proximal tubule in the rhesus monkey kidney decreased markedly from the first to the third segment. The mean values of the thinnest and thickest areas of the basement membrane of the third segment were compared with the same areas in the first and second segments. The significance of the differences was assessed using the non-paired T test; the difference in thickness of the basement membranes was highly significant ($p = <0.001$). Although it appears most valid to compare the thinnest areas of each segment since their thickness would be less influenced by tangential sectioning and other artifactual distortion, it is interesting to note that the thickest areas also showed the same significant differences. These findings emphasize the importance of identifying, as precisely as possible, the region of the proximal tubule under study in any investigation in which conclusions are being drawn regarding the significance of the thickness of the basement membrane. The functional significance of these findings awaits elucidation since very little is known about the possible physiologic role or capabilities of this structure in the proximal tubule.

A second significant finding was the effect of the method of fixative application on basement membrane thickness with certain fixatives. As shown in Table 4, the mean thicknesses of the thinnest and thickest areas of the basement membrane in the first segment of the proximal tubule were nearly identical using IVIP fixation with either osmium tetroxide or

glutaraldehyde. In addition, immersion fixation of renal tissue from the same animals in glutaraldehyde gave comparable results. However, in tissue which was immersion-fixed in osmium tetroxide, the average thickness of the basement membranes in the first segment was significantly greater (see Table 4). Such a finding is of considerable importance in studies in which conclusions regarding measurements of basement membrane thickness are made. The type of fixative and the method of application of the fixative must be taken into consideration in such studies.

Summary

The proximal tubule of the nondiseased kidney of the rhesus monkey (*Macaca mulatta*) was studied by light and electron microscopy. The morphology of the monkey proximal tubule was not found to be greatly different from that previously observed in the human kidney. The morphologic results obtained from immersion-fixed biopsy tissue were compared with those obtained by in-vivo intravascular perfusion fixation in the same animals using a variety of fixative and buffer combinations. Three distinct segments of the proximal tubule were identified on the basis of characteristic differences in their morphology. The mean thickness of the basement membrane of the proximal tubule decreased significantly from the first to the third segment. Basement membranes of tubules fixed by immersion in osmium tetroxide had a mean thickness significantly greater than that of tubules from the same animals preserved by in-vivo intravascular perfusion in the same fixative or in glutaraldehyde applied by immersion or perfusion. General cell shape, configuration, and organization were significantly altered in tissue fixed by immersion. Cellular organelles of immersion-fixed tissue, especially microbodies, exhibited marked distortion and morphologic alterations as compared to their counterparts in tubules preserved by *in vivo* intravascular perfusion. The possible pathophysiologic mechanism responsible for the alterations is discussed.

References

1. Bulger, R. E., and Trump, B. F. Fine structure of the rat renal papilla. *Amer J Anat 118*:685–721, 1966.
2. Ericsson, J. L. E. Absorption and decomposition of homologous hemoglobin in renal proximal tubule cells. An experimental light and electron microscopic study. *Acta Path Microbiol Scand (Suppl. 168)*:1–121, 1964.
3. Ericsson, J. L. E. and Trump, B. F. Electron microscopic studies of the epithelium of the proximal tubule of the rat kidney. I. The intracellular localization of acid phosphatase. *Lab Invest 13*:1427–1456, 1964.
4. Ericsson, J. L. E., Trump, B. F., and Weibel, J. Electron microscopic studies of the proximal tubule of the rat kidney. II. Cytosegresomes and

cytosomes: their relationship to each other and to the lysosome concept. *Lab Invest 14*:1341–1365, 1965.

5. ERICSSON, J. L. E., and TRUMP, B. F. Electron microscopic studies of the epithelium of the proximal tubule of the rat kidney. III. Microbodies, multivesicular bodies, and the Golgi apparatus. *Lab Invest 15*:1610–1633, 1966.
6. KURTZ, S. M. The fine structure of the lamina densa. *Lab Invest 10*:1189–1208, 1961.
7. LATTA, H., and MAUNSBACH, A. B. The juxtaglomerular apparatus as studied electron microscopically. *J Ultrastr Res 6*:547–561, 1962.
8. LATTA, H., and MAUNSBACH, A. B. Relations of the centrolobular region of the glomerulus to the juxtaglomerular apparatus. *J Ultrastr Res 6*:562–578, 1962.
9. MAUNSBACH, A. B. Observations on the segmentation of the proximal tubule in the rat kidney. *J Ultrastr Res 16*:239–258, 1966.
10. MAUNSBACH, A. B. Absorption of I^{125}-labelled homologous albumin by rat kidney proximal tubule cells. A study of microperfused single proximal tubules by electron microscope autoradiography and histochemistry. *J Ultrastr Res 15*:197–241, 1966.
11. MAUNSBACH, A. B., MADDEN, S. C., and LATTA, H. Variations in fine structure of renal tubular epithelium under different conditions of fixation. *J Ultrastr Res 6*:511–530, 1962.
12. PEASE, D. C. Electron microscopy of the tubular cells of the kidney cortex. *Anat Rec 121*:723–744, 1955.
13. OSVALDO, L., and LATTA, H. The thin limbs of the loop of Henle. *J Ultrastr Res 15*:144–168, 1966.
14. OSVALDO, L., and LATTA, H. Interstitial cells of the renal medulla. *J Ultrastr Res 15*:589–613, 1966.
15. RHODIN, J. Correlation of ultrastructural organization and function in normal and experimentally changed proximal convoluted cells of the mouse kidney. (Thesis, Karolinska Institutet, Stockholm). Aktiebolaget Godvil, Stockholm, 1954.
16. RHODIN, J. Anatomy of kidney tubules. *Intern Rev Cytol 7*:485–534, 1958.
17. TRUMP, B. F., and ERICSSON, J. L. E. The effect of the fixative solution on the ultrastructure of cells and tissues. A comparative analysis with particular attention to the proximal convoluted tubule of the rat kidney. *Lab Invest 14*:1245–1323, 1965.
18. LATTA, H., MAUNSBACH, A. B., and OSVALDO, L. The fine structure of renal tubules in cortex and medulla. In *Ultrastructure of the Kidney*, DALTON, A. J., and HAGUENAU, F. Eds. Acad Press, New York, 1967, pp. 2–45.
19. TRUMP, B. F., and BULGER, R. E. The morphology of the kidney. In *The Structural Basis of Renal Disease*, BECKER, E. L. Ed. Hoeber, New York, 1968, pp. 1–92.
20. GRIFFITH, L. D., BULGER, R. E., and TRUMP, B. F. The ultrastructure of the functioning kidney. *Lab Invest 16*:220–246, 1967.
21. BERGSTRAND, A., and BUCHT, H. Anatomy of the glomerulus as observed in biopsy material from young and healthy human subjects. *Z Zellforsch 48*:51–73, 1958.

22. BERGSTRAND, A., and ERICSSON, J. Elektronmikroskopisk undersokning av tubulusepitelet has friska manniskor. *Nord Med 64*:1047, 1960.

23. TISHER, C. C., BULGER, R. E., and TRUMP, B. F. Human renal ultrastructure. I. Proximal tubule of healthy individuals. *Lab Invest 15*:1357–1396, 1966.

24. BULGER, R. E., TISHER, C. C., MYERS, C. H., and TRUMP, B. F. Human renal ultrastructure. II. The thin limb of Henle's loop and the interstitium in healthy individuals. *Lab Invest 16*:124–141, 1967.

25. TISHER, C. C., BULGER, R. E., and TRUMP, B. F. Human renal ultrastructure. III. The distal tubule in healthy individuals. *Lab Invest 18*:655–668, 1968.

26. MYERS, C. H., BULGER, R. E., TISHER, C. C., and TRUMP, B. F. Human renal ultrastructure. IV. Collecting duct of healthy individuals. *Lab Invest 15*:1921–1950, 1966.

27. ERICSSON, J. L. E., BERGSTRAND, A., ANDRES, G., BUCHT, H., and CINOTTI, G. Morphology of the renal tubular epithelium in young, healthy humans. *Acta Path Microbiol Scand 63*:361–384, 1965.

28. ERICSSON, J. L. E., ANDRES, G., BERGSTRAND, A., BUCHT, H., and OBSTEN, P. Further studies on the fine structure of renal tubules in healthy humans with a note on the effect of the intravenous infusion of low molecular weight dextran. *Acta Path Microbiol Scand 69*:493–513, 1967.

29. TISHER, C. C., FINKEL, R. M., ROSEN, S., and KENDIG, E. M. Renal microbodies in the rhesus monkey. *Lab Invest 19*:1–6, 1968.

30. ROSEN, S., and TISHER, C. C. Observations on the rhesus monkey glomerulus and juxtaglomerular apparatus. *Lab Invest 18*:240–248, 1968.

31. TISHER, C. C. Morphology of the chimpanzee kidney: A comparison with man. In *Handbook of the Chimpanzee*, BOURNE, G. H., Ed. Karger, New York. In Press.

32. BARAJAS, L. The innervation of the juxtaglomerular apparatus; An electron microscopic study of the innervation of the glomerular arterioles. *Lab Invest 13*:916–929, 1964.

33. BARAJAS, L. The development and ultrastructure of the juxtaglomerular cell granule. *J Ultrastr Res 15*:400–413, 1966.

34. LUFT, J. H. Improvements in epoxy resin embedding methods. *J Biophys Biochem Cytol 9*:409–414, 1961.

35. WATSON, M. L. Staining of tissue sections for electron microscopy with heavy metals. II. Application of solutions containing lead and barium. *J Biophys Biochem Cytol 4*:727–730, 1958.

36. REYNOLDS, E. S. The use of lead citrate at high pH as an electron-opaque stain in electron microscopy. *J Cell Biol 17*:208–212, 1963.

37. LILLIE, R. D. *Histopathologic Technique and Practical Histochemistry*. Blakiston, New York, 1954.

38. TRUMP, B. F., SMUCKLER, E. A., and BENDITT, E. P. A method for staining epoxy sections for light microscopy. *J Ultrastr Res 5*:343–348, 1961.

39. HRUBAN, Z., and RECHCIGL, M., Jr. Comparative ultrastructure of microbodies. *Fed Proc 26*:513, 1967.

40. ROBINSON, F. R., and ZIEGLER, R. F. Clinical laboratory data derived from 102 Macaca mulatta. *Lab Animal Care 18*:50–57, 1968.

41. PETERY, J. J. Ultramicroanalysis of selected blood components of normal Macaca mulatta. *Lab Animal Care 17*:342–344, 1967.

42. MELVILLE, G. S., JR., WHITCOMB, W. H., and MARTINEZ, R. S. Hematology of the Macaca mulatta monkey. *Lab Animal Care* 17:189–198, 1967.

43. KING, T. O., and GARGUS, J. L. Normal blood values of the adult female monkey (Macaca mulatta). *Lab Animal Care* 17:391–396, 1967.

44. ANDERSON, D. R. Normal values for clinical blood chemistry tests of the Macaca mulatta monkey. *Amer J Vet Res* 27:1484–1489, 1966.

45. SMITH, H. W., and CLARKE, R. W. The excretion of inulin and creatinine by the anthropoid apes and other infrahuman primates. *Amer J Physiol* 122:132–139, 1938.

46. STAHL, W. R., and MALINOW, M. R. A survey of physiological measurements in Macaca mulatta. *Folia Primat* 7:12–33, 1967.

47. PICKERING, D. E., and SUSSMAN, H. H. Renal function studies in monkeys (Macaca mulatta). *Amer J Vet Res* 23:667–672, 1962.

48. LONGLEY, J. B., and BURSTONE, M. S. Intraluminal nuclei and other inclusions as agonal artifacts of the renal proximal tubules. *Amer J Path* 42: 643–655, 1963.

49. TRUMP, B. F., and BULGER, R. E. Studies of cellular injury in isolated flounder tubules I. Correlation between morphology and function of control tubules and observations of autophogy and mechanical cell damage. *Lab Invest* 16:453–482, 1967.

50. TRUMP, B. F., and BULGER, R. E. Studies of cellular injury in isolated flounder tubules. III. Light microscopic and functional changes due to cyanide. *Lab Invest* 18:721–730, 1968.

51. TRUMP, B. F., and BULGER, R. E. Studies of cellular injury in isolated flounder tubules. IV. Electron microscopic observations of changes during the phase of altered homeostasis in tubules treated with cyanide. *Lab Invest* 18:731–739, 1968.

52. TRUMP, B. F., and GINN, F. L. Studies of cellular injury in isolated flounder tubules. II. Cellular swelling in high potassium media. *Lab Invest* 18:341–351, 1968.

53. SUZUKI, T. Zur Morphologie der Nierensekretion unter physiologischen und pathologischen Beding ungen. Jena, Fischer, 1912.

54. SJOSTRAND, F. X. Uber die Eigenfluoreszenz tierischer Gewebe mit besondrer Berucksichtigung der Saugetierniere. *Acta Anat (Suppl. 1)* 1:1–163, 1945–1946.

55. BATELLI, F., and STERN, L. Untersuchungen uber die urikase in den tiergeweben. *Biochem Z* 19:219–253, 1909.

56. GRAFFLIN, A. L., and FOOTE, J. J. Epithelial cell shapes in first segment of the proximal tubule of cat nephron, as demonstrated by chrome-silver method. *Amer J Anat* 65:179–198, 1939.

57. MUGNAINI, E. Helical filaments in astrocytic mitochondria of the corpus striatum in the rat. *J Cell Biol* 23:173–182, 1964.

58. ISERI, O. A., LIEBER, C. S., and GOTTLIEB, L. S. The ultrastructure of fatty liver induced by prolonged ethanol ingestion. *Amer J Path* 48:535–555, 1966.

59. PORTA, E. A., HARTROFT, W. S., and DE LA IGLESIA, F. A. Hepatic changes associated with chronic alcoholism in rats. *Lab Invest* 14:1437–1455, 1965.

60. SVOBODA, D. J., and HIGGINSON, J. Ultrastructural changes produced by protein and related deficiencies in the rat liver. *Amer J Path* 45:353–380, 1964.

61. SUZUKI, T., and MOSTOFI, F. K. Intramitochondrial filamentous bodies in the thick limb of Henle of the rat kidney. *J Cell Biol* 33:605–623, 1967.

The authors wish to express their gratitude to Mr. John McClain of the Medical Audio Visual Department and to Mrs. Loutisha Templeman of the Department of Metabolism, Walter Reed Army Institute of Research, Washington D.C. 20012.

[*Illustrations follow*]

Legends for Figures

Key:

AL	Ascending thick limb of Henle's loop	IM	Interstitium
AV	Apical vacuole	IS	Intercellular space
BB	Brush border	L	Lipid
BM	Basement membrane	Lf	Lipofuscin
BS	Bowman's space	M	Mitochondrion
C	Cytosome	Mb	Microbody
Cap	Capillary	MvB	Multivesicular body
Cs	Cytosergresome (autophagic vacuole)	N	Nucleus
DT	Apical dense tubule	PT	Proximal tubule
Go	Golgi complex	RBC	Red blood cell
HL	Descending thin limb of Henle's loop	TL	Tubular lumen
IC	Interstitial cell	V	Apical vesicle
		VC	Visceral epithelial cell
		Ve	Vessel

All light micrographs represent 0.5–1.0 μ sections of tissue embedded in Epon epoxy resin and stained with toluidine blue.[38] Tissue represented in Fig 1, 2, 4, and 5 was fixed by IVIP in 2% osmium tetroxide buffered in 0.1 M s-collidine. Tissue represented in Fig 3 and 29 was fixed by IVIP in 1% osmium tetroxide buffered in phosphate. Tissue pictured in Fig 28 was fixed by immerson in 6.25% glutaraldehyde buffered in 0.1 M sodium cacodylate and post-fixed in 1% osmium tetroxide in phosphate buffer.

Fig 6, 7, 13, 14, 17, 21, and 36 are electron micrographs of tissue fixed by IVIP with 1% osmium tetroxide in phosphate buffer. Fig 8, 9, 15, 16, 18, and 23–27 are electron micrographs of tissue fixed by IVIP in 2% osmium tetroxide buffered in 0.1 M s-collidine. Fig 10 and 11 were fixed by IVIP in 6.25% glutaraldehyde buffered in 0.1 M sodium cacodylate and post-fixed in 2% osmium tetroxide in 0.1 M s-collidine. Fig 12 and 30 represent tissue fixed by immersion in 1% osmium tetroxide buffered in phosphate. Fig 19, 20, 22, and 35 represent tissue fixed by IVIP with 6.25% glutaraldehyde buffered in 0.1 M sodium cacodylate and post-fixed in 1% osmium tetroxide in phosphate buffer. Fig 31 and 37–39 represent tissue fixed in 2% glutaraldehyde in sodium cacodylate buffer. Fig 32 and 34 represent tissues fixed by immersion in 6.25% glutaraldehyde buffered in 0.1 M sodium cacodylate and post-fixed in 1% osmium tetroxide in phosphate buffer. All sections were stained with uranyl acetate and lead citrate as described in the methods section.

Fig 1. Light micrograph depicting abrupt transition *(arrow)* from lowlying squamous epithelium lining Bowman's capsule to tall columnar epithelium characteristic of first segment of proximal tubule. × 500.

Fig 2. Light micrograph of first segment of proximal tubule. Epithelium is tall and columnar, brush border is well developed, and cells are packed with elongate mitochondria. × 700.

Fig 3. Light micrograph showing portions of three adjacent tubules characteristic of second segment of proximal tubule. Large accumulations of lipid droplets *(arrows)* near cell base distinguish this segment from other regions of proximal tubule. × 950.

Fig 4. Light micrograph depicting third segment of proximal tubule. Cells are cuboidal in shape and contain fewer organelles than first two segments. × 950.

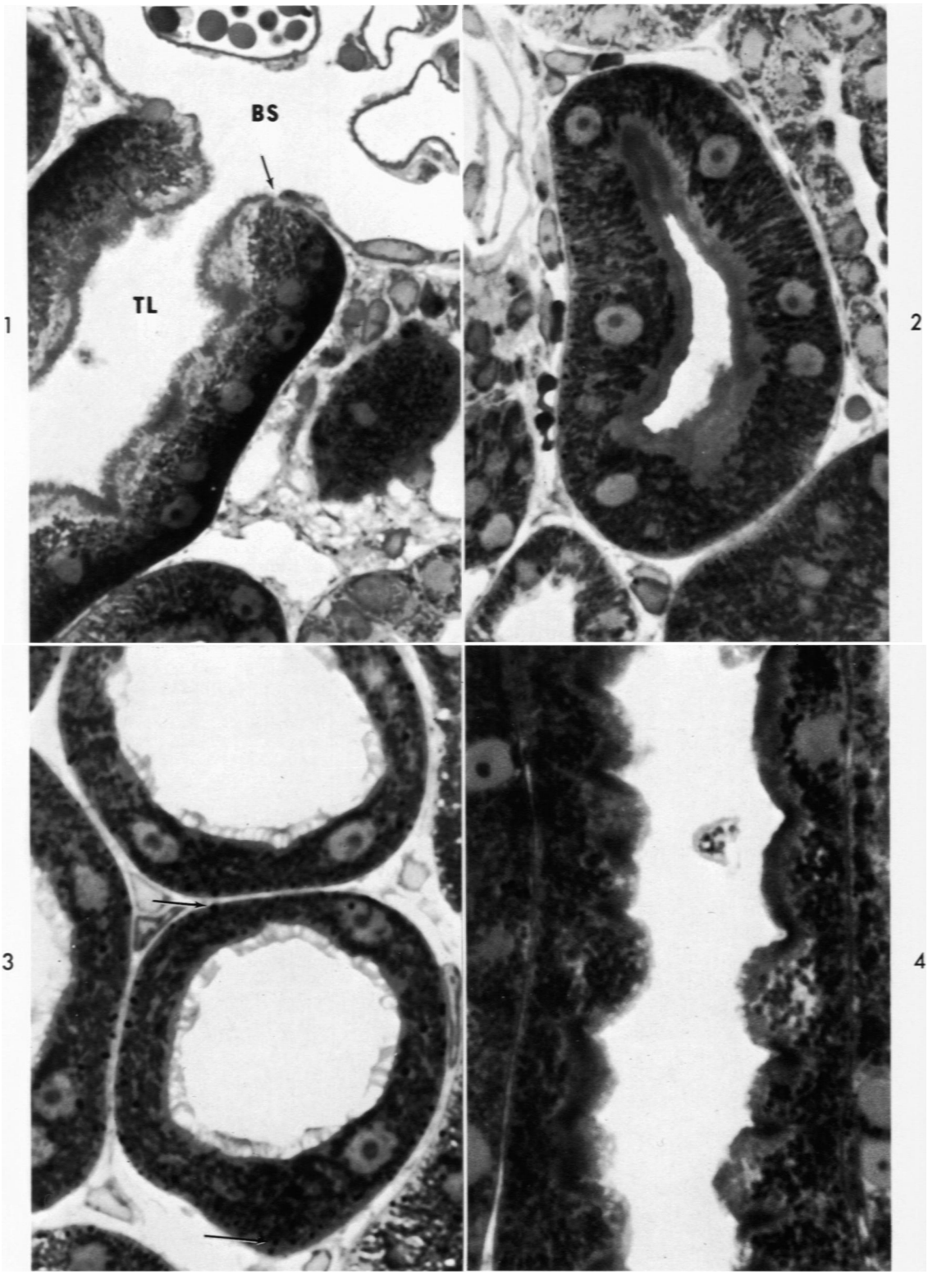
BS
TL
1
2
3
4

Fig 5. Light micrograph showing characteristic gradual transition from terminal proximal tubule on right to early descending thin limb of Henle's loop on left. × 740.

Fig 6. Electron micrograph demonstrating transition from squamous epithelium (*arrow*) lining Bowman's capsule to columnar cells of the proximal tubule at left. × 6400.

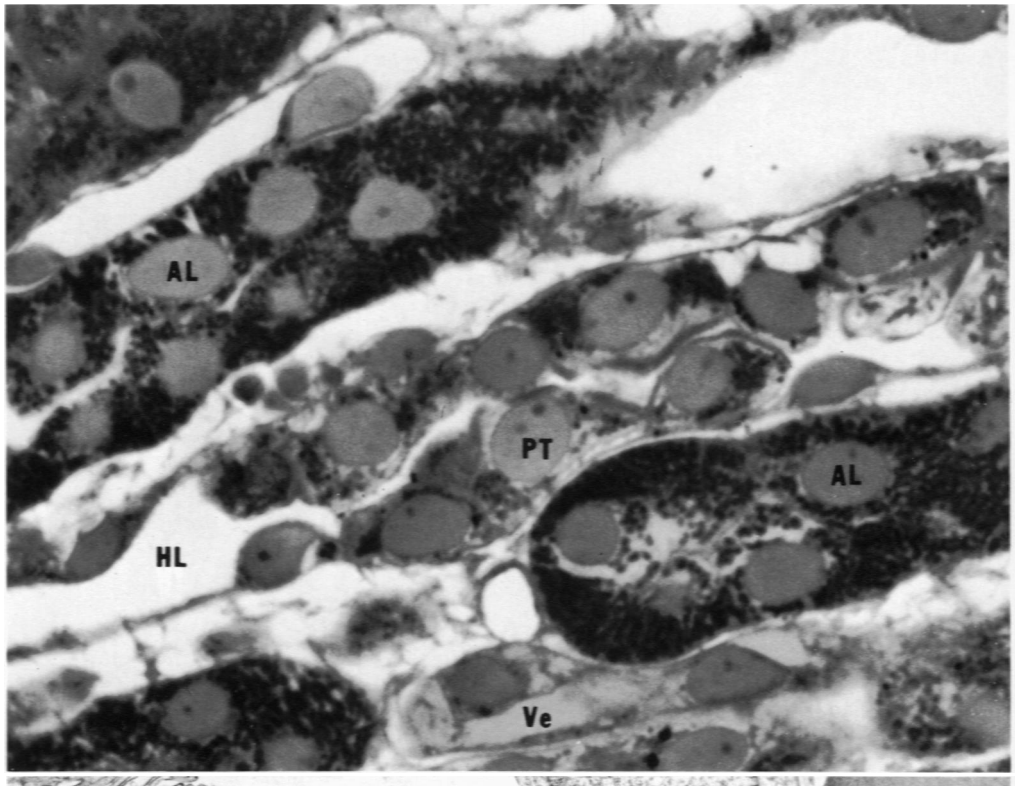

5

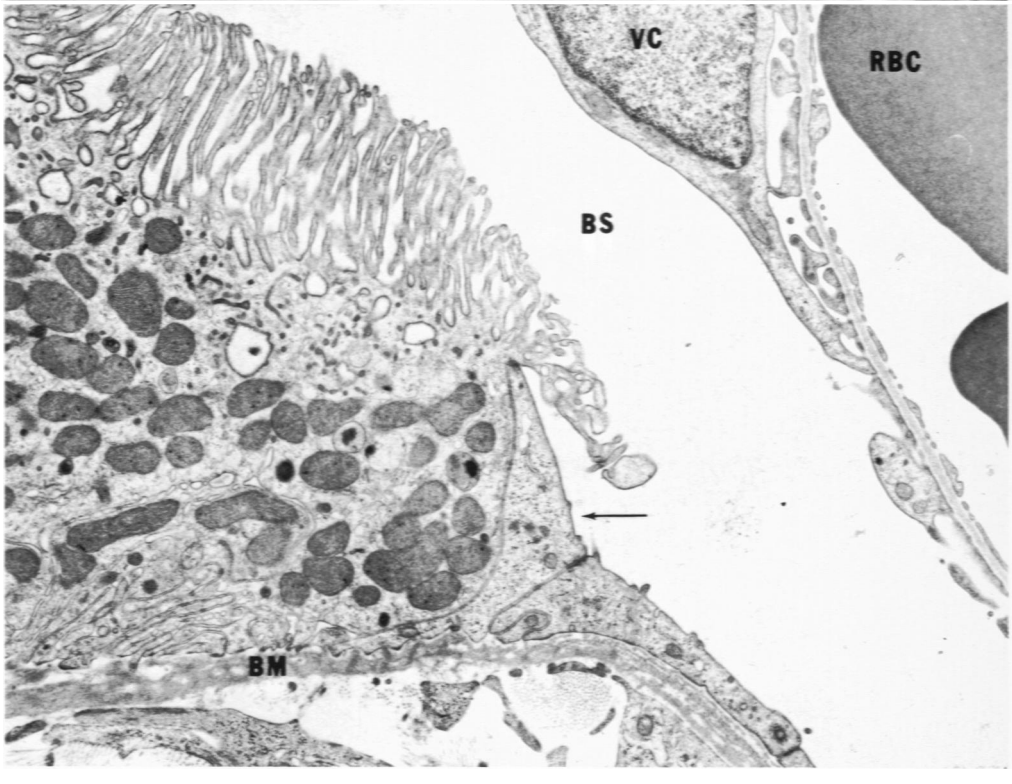

6

Fig 7. Electron micrograph of typical tall columnar cell from first segment of proximal tubule. Elongate mitochondrial profiles (*M*) are enclosed within plications of basal plasmalemma. Apical system of vesicles, vacuoles, and dense tubules is well developed. × 9165.

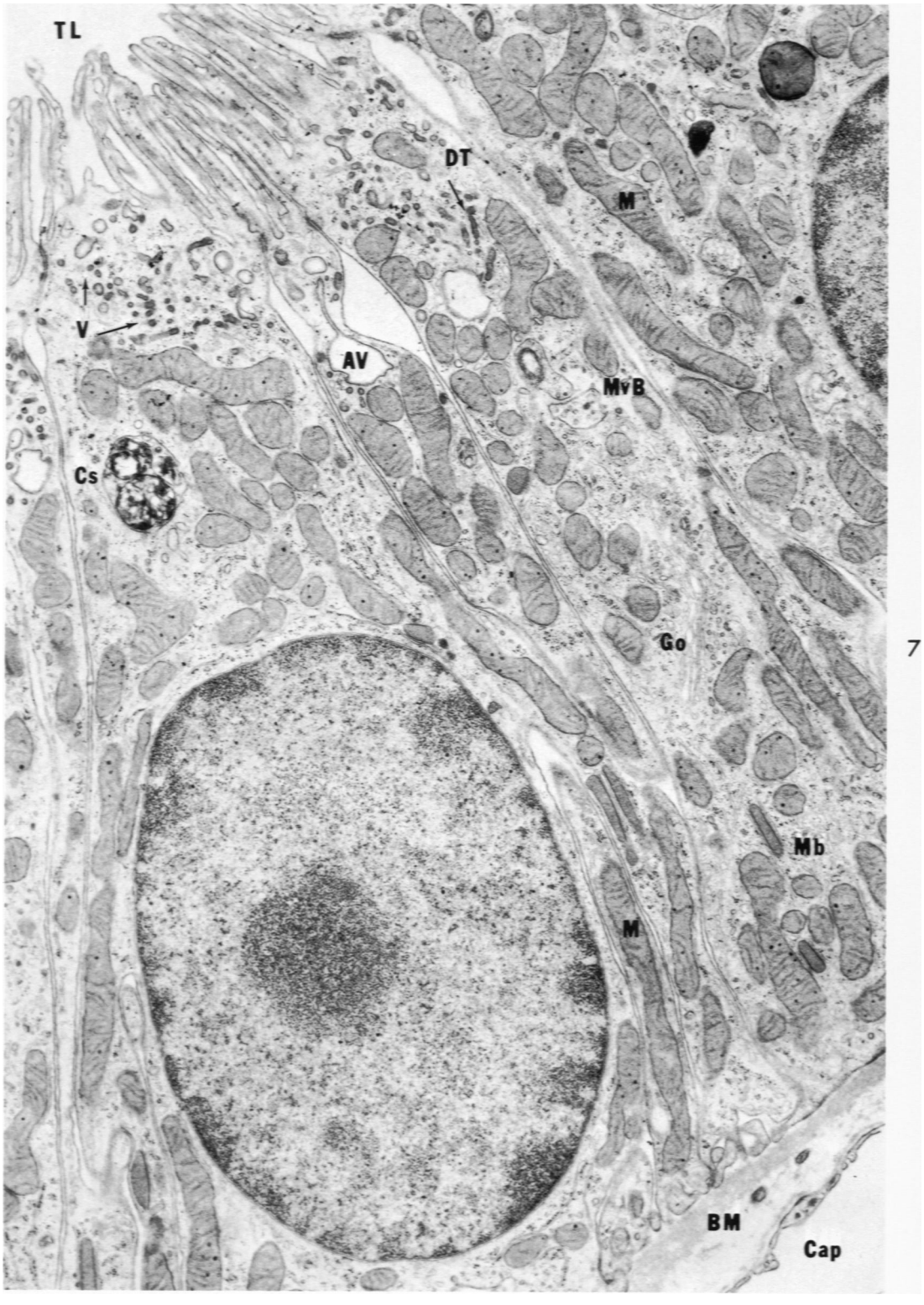
TL
DT
M
V
AV
MvB
Cs
Go
Mb
M
BM
Cap

Fig 8. Higher power electron micrograph demonstrating complex interdigitations of adjacent proximal tubule cells. Note that as in other mammals, mitochondrial profiles are inclosed within plications of basal plasmalemma, and true basilar infoldings where the infolded plasma membrane returns to the original point of inflection do not exist. × 14,280.

Fig 9. Electron micrograph depicting evagination or outpouching at base of proximal tubule cell. Such structures were observed in both first and second segments of proximal tubule in perfusion-fixed tissue. Bands of coarse fibrils (*arrow*) usually extended across mouth of these evaginations running parallel to adjacent basement membrane. × 14,075.

Fig 10. Higher power electron micrograph to show appearance of several structures within apical cell region. Two types of apical vesicles are present. First type (*arrows*) is smaller and exhibits an organized internal lining of short filaments resembling glycocalyx of apical cell membrane; externally there is a coating of radially directed short bristles. Second type of apical vesicle is slightly larger, possesses dense internal lining and often internal limiting membrane. Dense tubules are frequently seen in direct connection with larger apical vesicle. × 32,700.

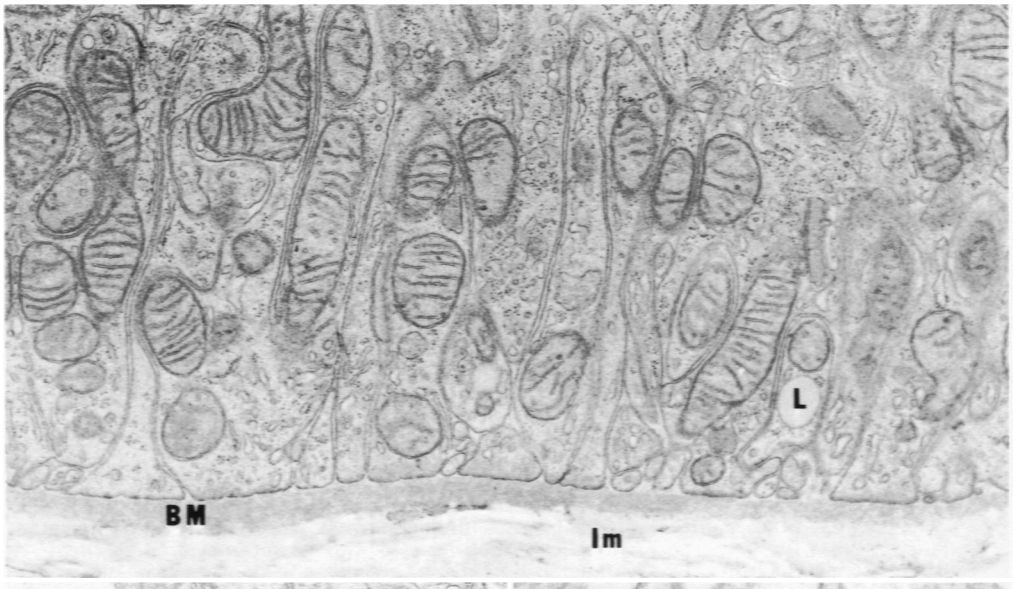

8

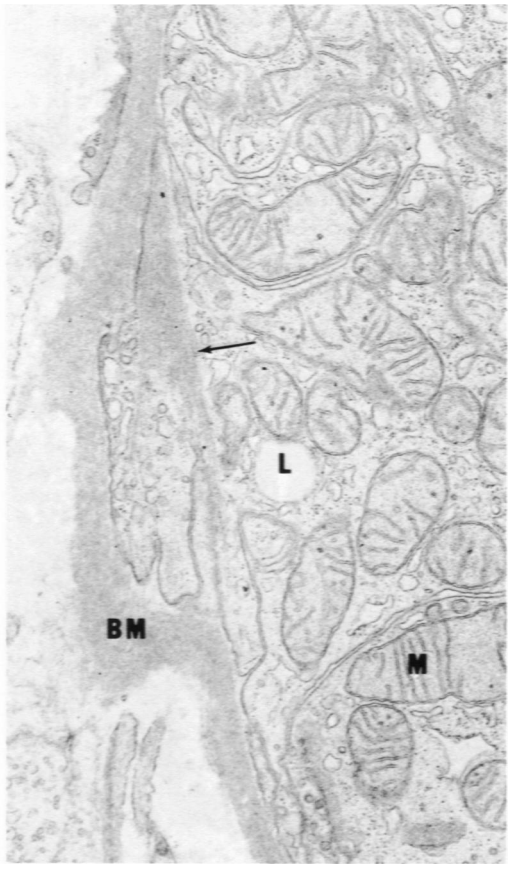

9

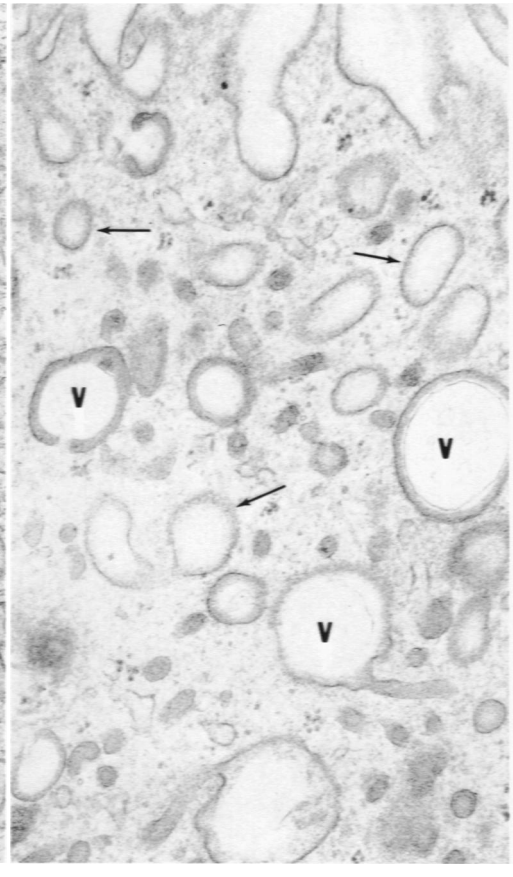

10

Fig 11. High power electron micrograph showing connection between apical vesicle with dense internal lining and apical dense tubule. Several cross sections of apical dense tubules are also shown. Smaller apical vesicles with no internal limiting membrane but with external radially-directed bristle coat are present along right of picture. × 56,650.

Fig 12. Electron micrograph showing portions of apical regions of two adjacent proximal tubule cells separated by intercellular space. Apical dense tubules (*arrows*) are shown opening into lateral intercellular space. Apical vacuole with a connecting dense tubule is present on left. Such a finding may represent another pathway for transport of colloidal materials from tubular lumen to peritubular capillaries. × 41,600.

Fig 13. Electron micrograph showing cluster of elongate microbodies in first segment of proximal tubule. Each organelle possesses one or two dense marginal plates contiguous with adjacent endoplasmic reticulum. × 71,500.

Fig 14. High power electron micrograph demonstrating layering of marginal plates of two adjacent microbodies (*arrows*). Marginal plates often exhibited definite periodicity suggesting presence of internal structure. × 81,100.

Fig 15. High power electron micrograph demonstrating presence of definite internal structure within marginal plates (*arrow*) of microbody. Regular periodicity of 125 A was present in this marginal plate. × 166,000.

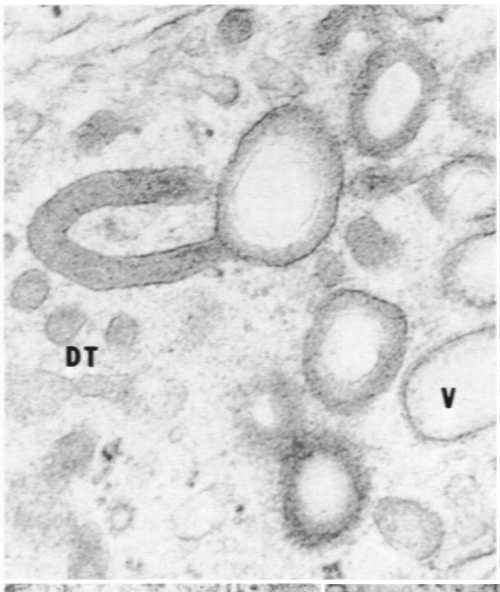

11

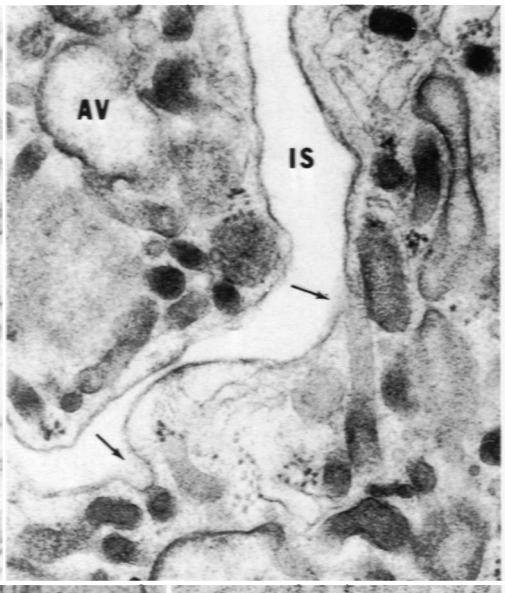

12

13

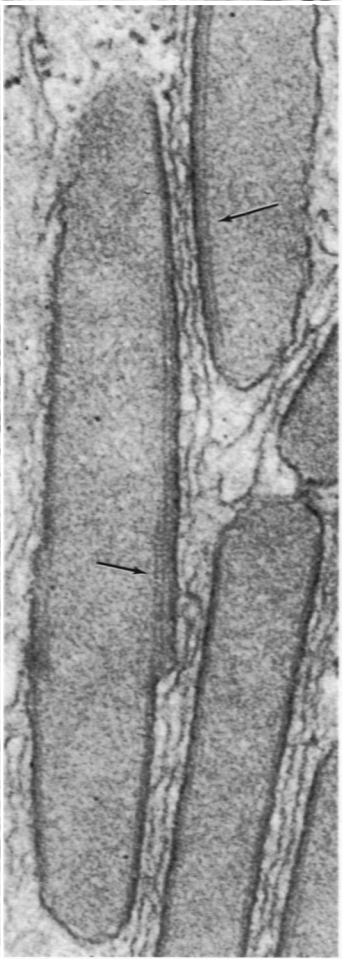

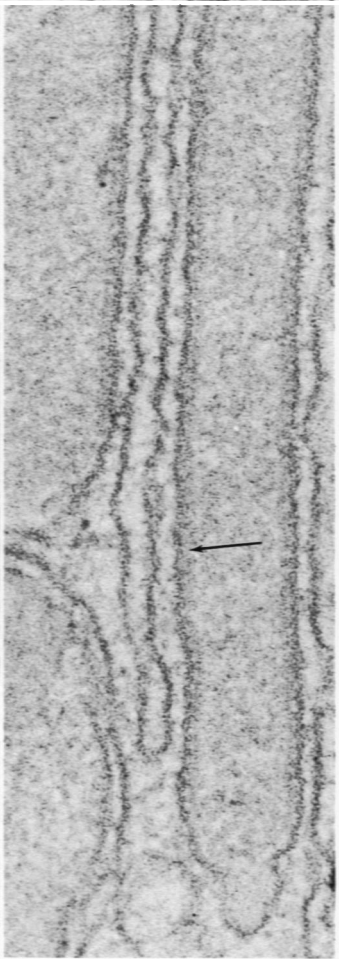

14,15

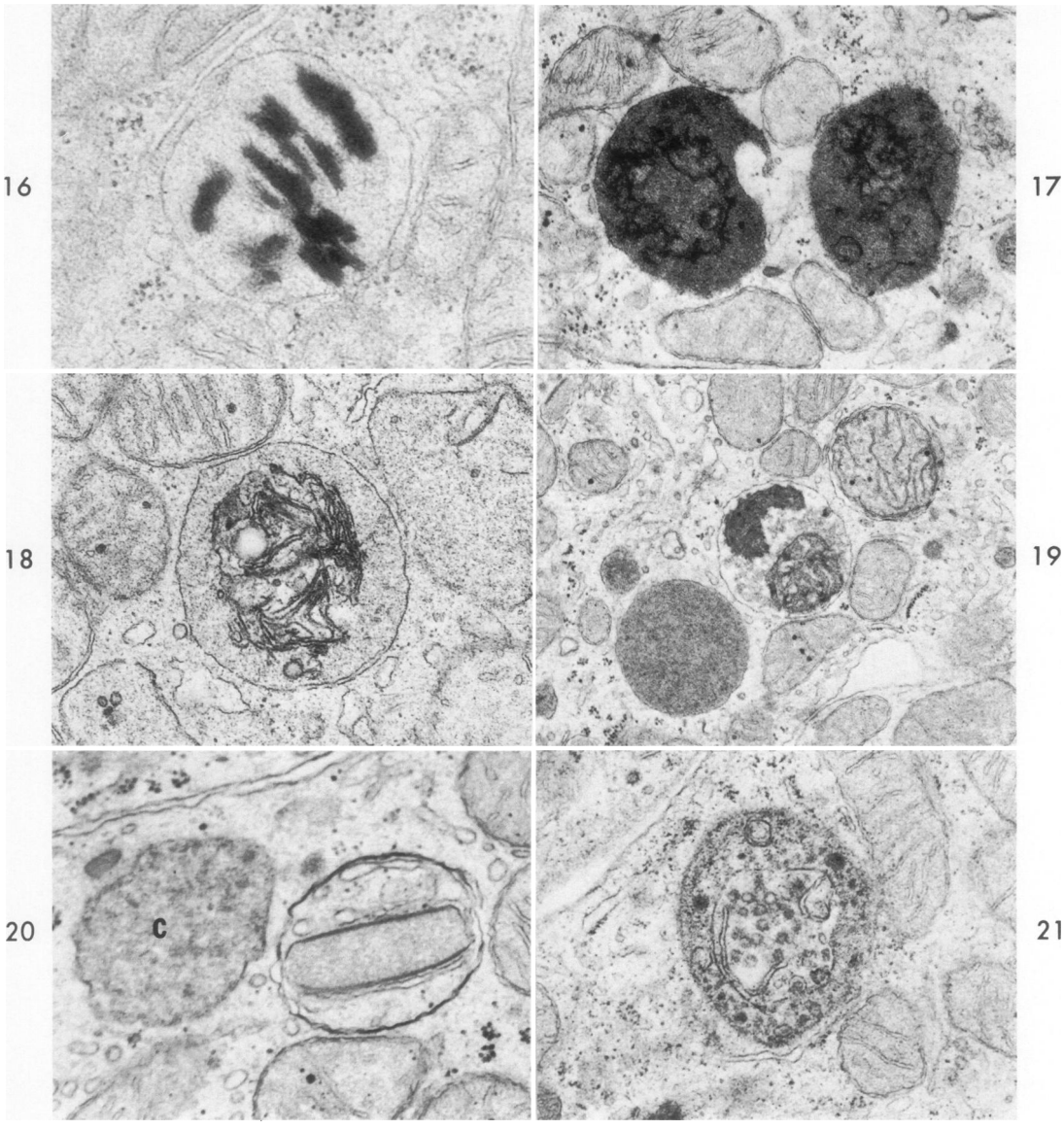

Fig 16. Electron micrograph of cytosome characteristic of early first segment of proximal tubule. × 43,250.

Fig 17. Electron micrograph showing two adjacent dense cytosomes containing membrane-like fragments. This tissue was fixed by IVIP in 1% osmium tetroxide in phosphate buffer. × 25,000.

Fig 18. Electron micrograph of cytosome which is similar in structure and content to those pictured in Fig 17 but exhibits pale background matrix. Fixation in this case was accomplished by IVIP with osmium tetroxide in *s*-collidine buffer. × 28,200.

Fig 19. Electron micrograph of portion of proximal tubule cell fixed in 6.25% glutaraldehyde. Cytosome at lower left is dense and homogeneous in appearance. Two cytosegresomes (autophagic vacuoles) which contain mitochondria undergoing breakdown are pictured at right. × 19,400.

Fig 20. Electron micrograph of a cytosegresome containing microbody and fragments of smooth endoplasmic reticulum. Cytosome is present at left. × 31,100.

Fig 21. Electron micrograph of cytosegresome containing mixed cellular debris. × 30,600.

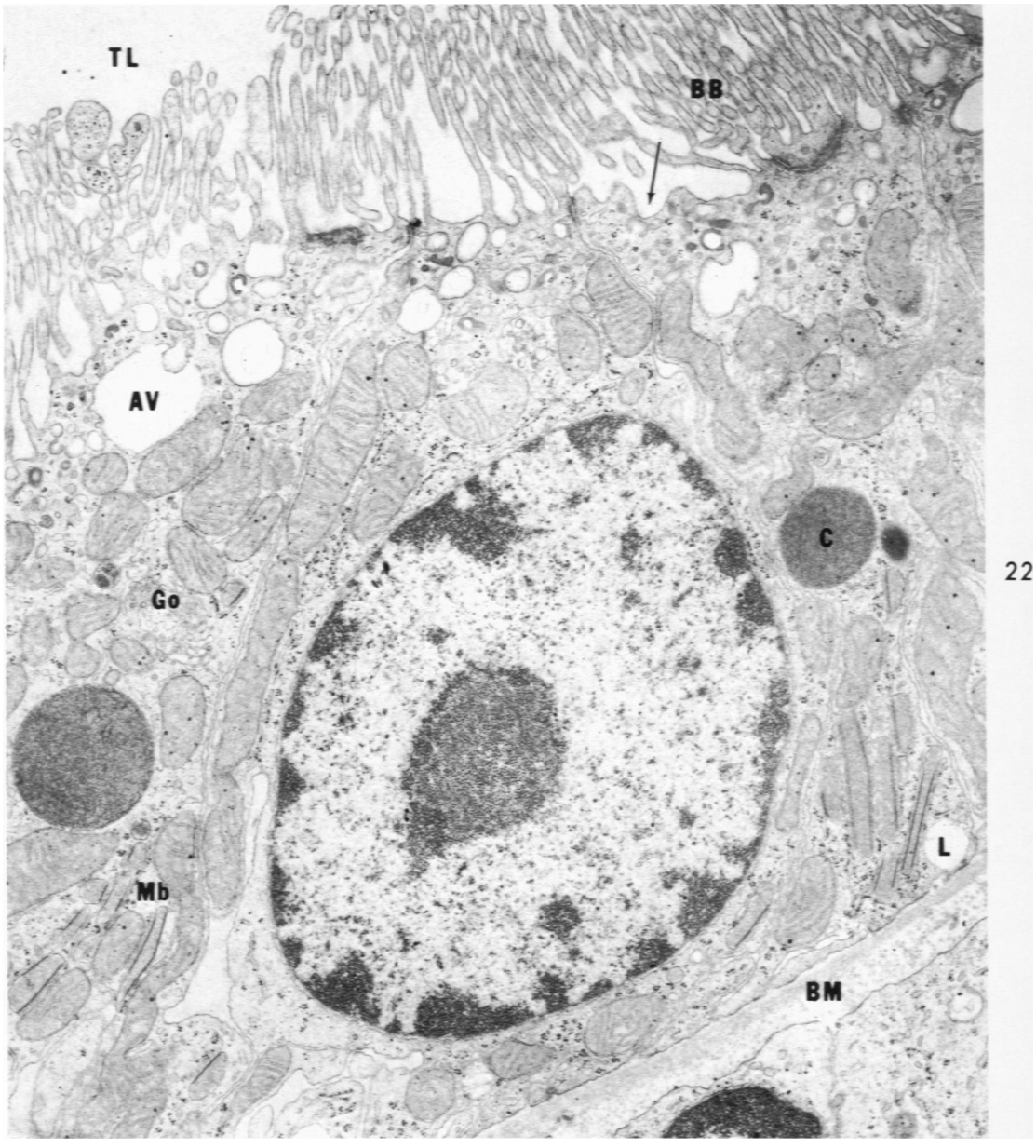

22

Fig 22. Low power electron micrograph of proximal tubule cell characteristic of second segment. Brush border is more irregular than that of first segment with occasional skip areas (*arrow*) being present. Apical vesicles and dense tubules are not as extensively developed but apical vacuoles are often more prominent. Cell is low columnar and lateral interdigitations with adjacent cells are less complex. × 8900.

Fig 23. Low power electron micrograph showing proximal tubule cell characteristic of third segment. Cells are cuboidal and exhibit a well-developed brush border. Apical dense tubules and apical vacuoles are not extensive in this segment, although small apical vesicles are abundant. Microbodies were the most common SMLIB in this segment. Note the very thin basement membrane. × 11,000.

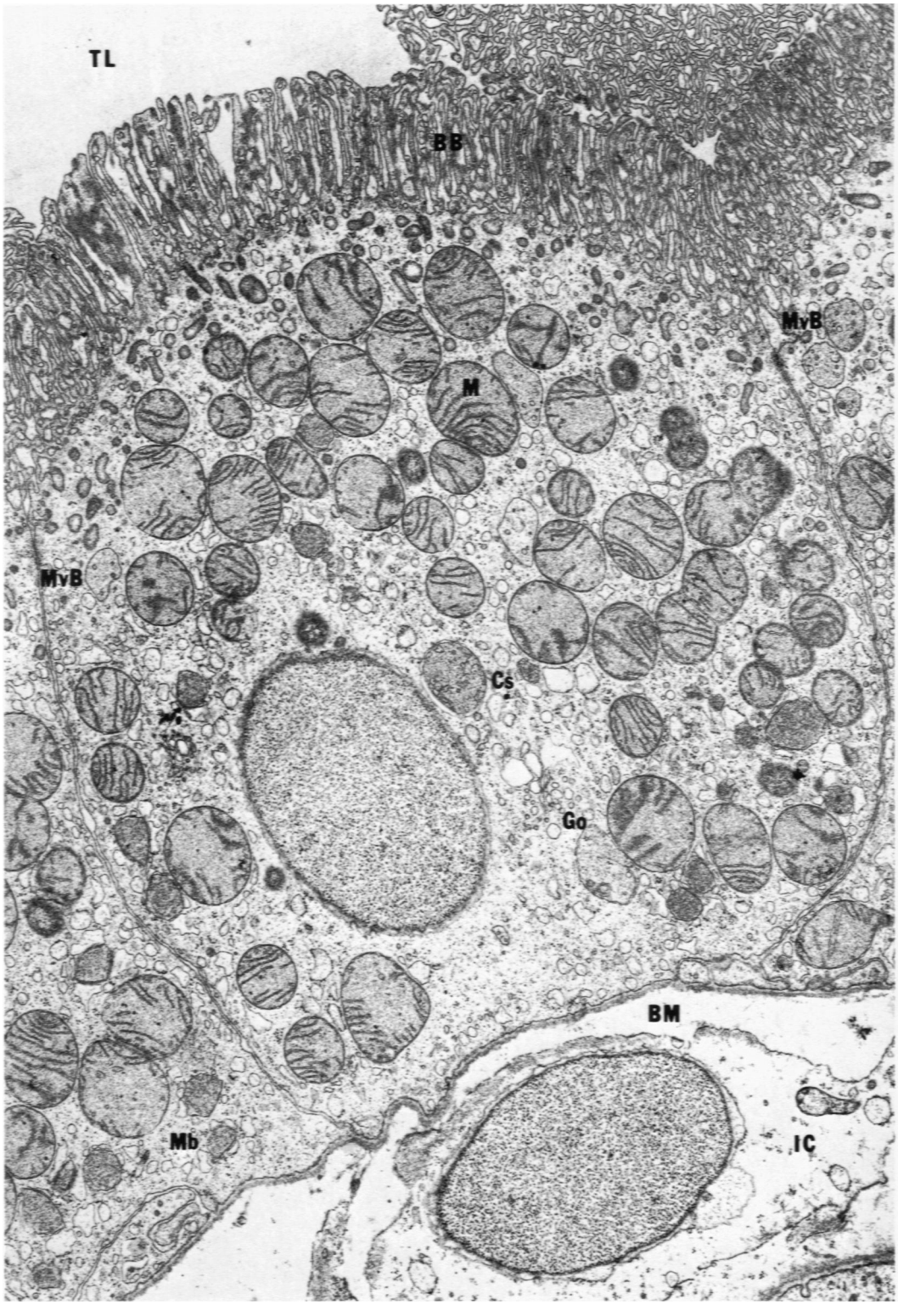

23

Fig 24. Electron micrograph showing apical region of proximal tubule cell characteristic of third segment. Multivesicular bodies are abundant in this segment, especially near cell apex, and are often extremely variable in size and shape. Note absence of microvilli (*arrow*) over short segment of apical plasmalemma. × 9950.

Fig 25. Higher power electron micrograph showing cluster of microbodies. A possible connection between labelled microbody and endoplasmic reticulum is shown. × 30,700.

Fig 26. Electron micrograph of proximal tubule cell near transition into thin descending limb of Henle containing large accumulations of lipofuscin. This is a characteristic feature in this region. × 12,650.

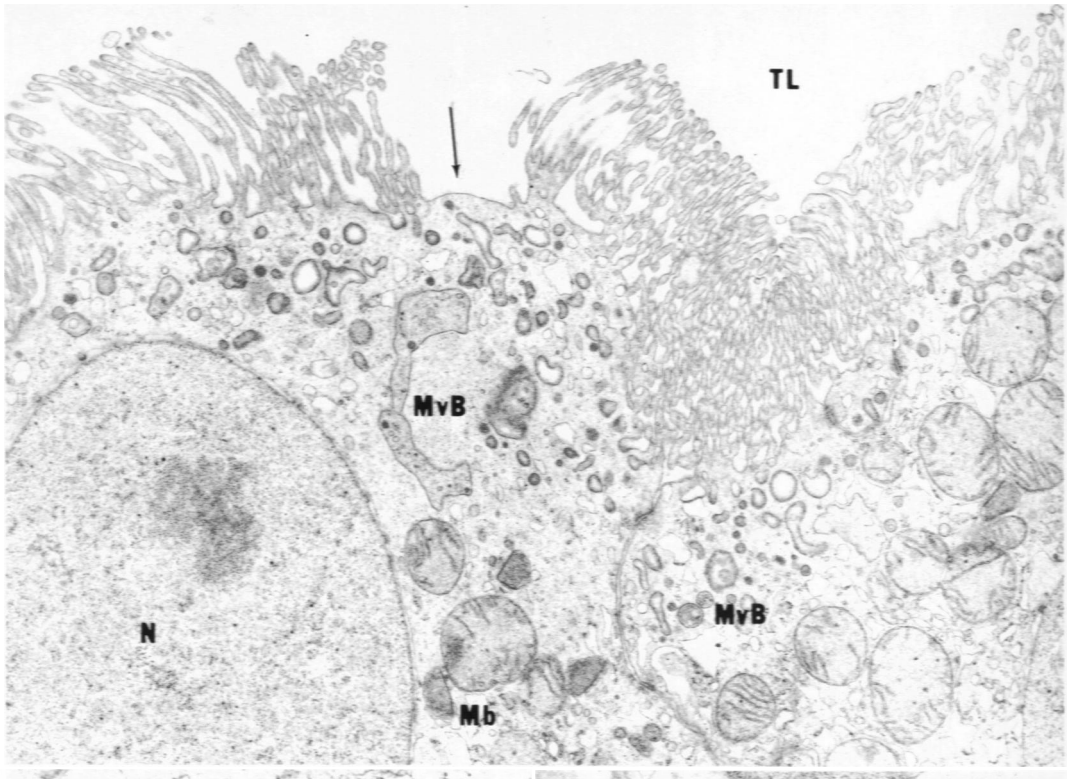

24

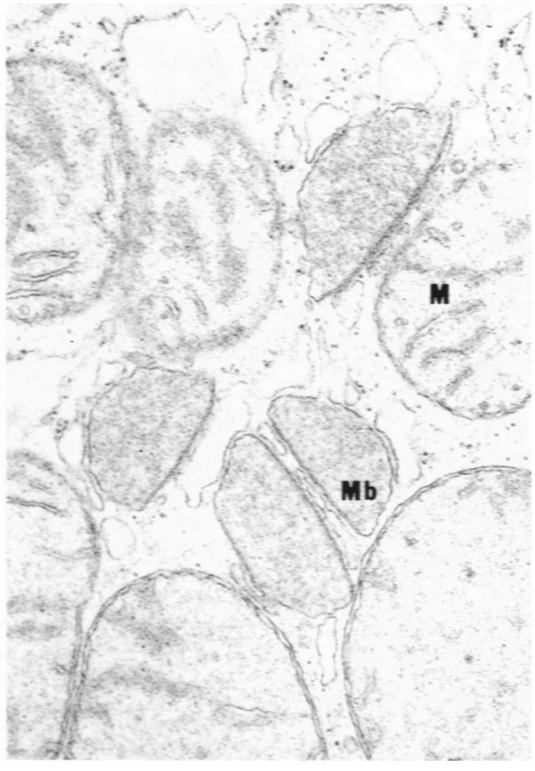

25

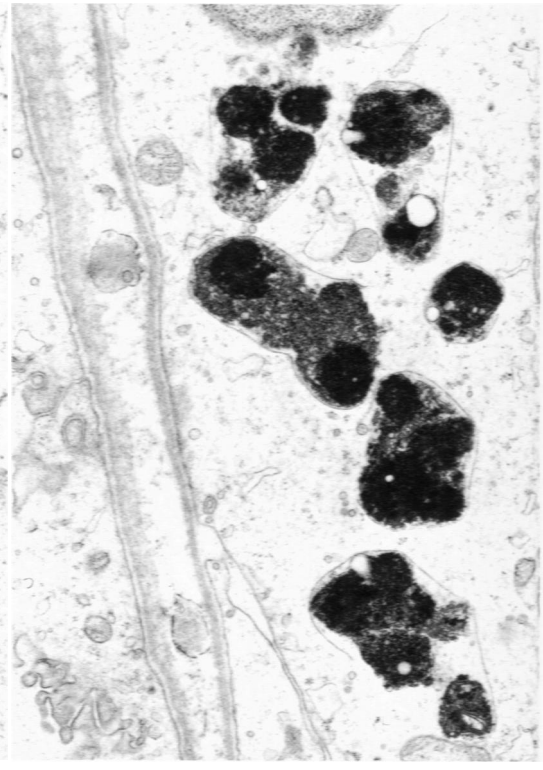

26

Fig 27. Electron micrograph of transition region between proximal tubule and thin limb showing terminal proximal tubule cells, above, and cells of the early descending thin limb of Henle's loop, below. Absence of microvilli (*arrows*) over large areas of the apical cell surface was characteristic of this region of proximal tubule. Note particularly the uniformly thin basement membrane. × 6250.

Fig 28. Light micrograph of proximal tubule characteristic of tissue fixed by immersion. Note completely occluded tubular lumen and greatly widened extracellular spaces (*arrows*). Compare these findings with Fig 29 which represents proximal tubules from areas of kidneys unsuccessfully preserved by IVIP. × 625.

Fig 29. Light micrograph of proximal tubules from area of kidney not successfully preserved by IVIP. Note that tubular lumens are nearly totally occluded. Lateral intercellular spaces between cells (*arrows*) are greatly widened resembling renal tissue fixed by immersion, as shown in Fig 28. × 660.

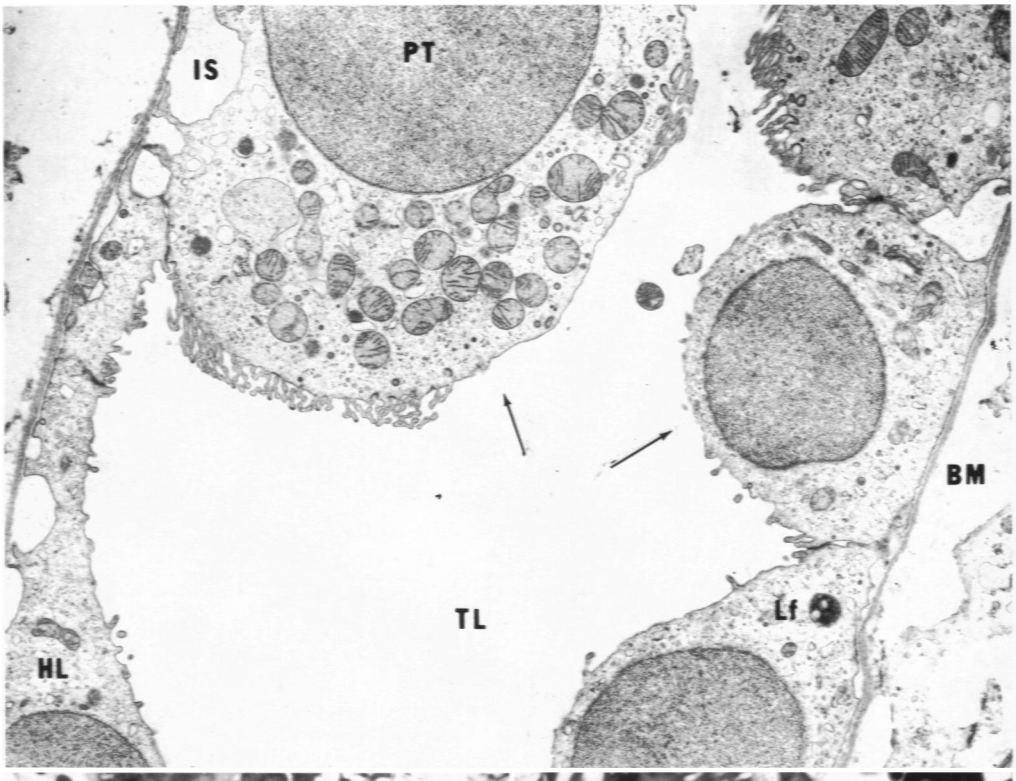

27

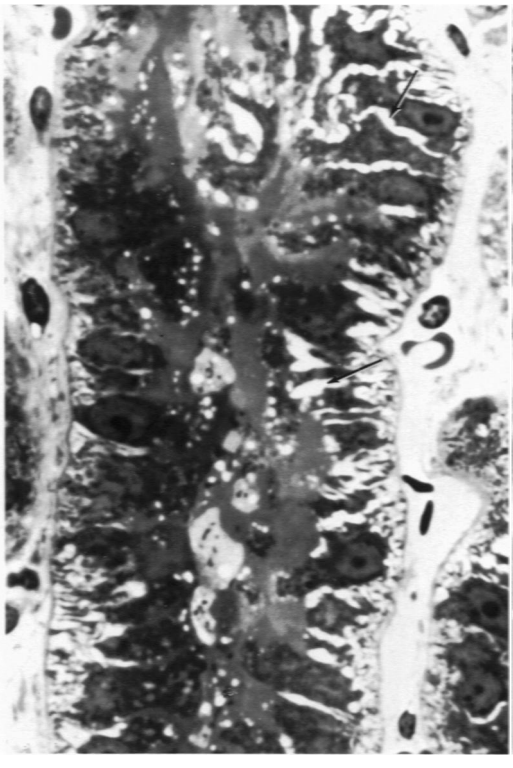

28

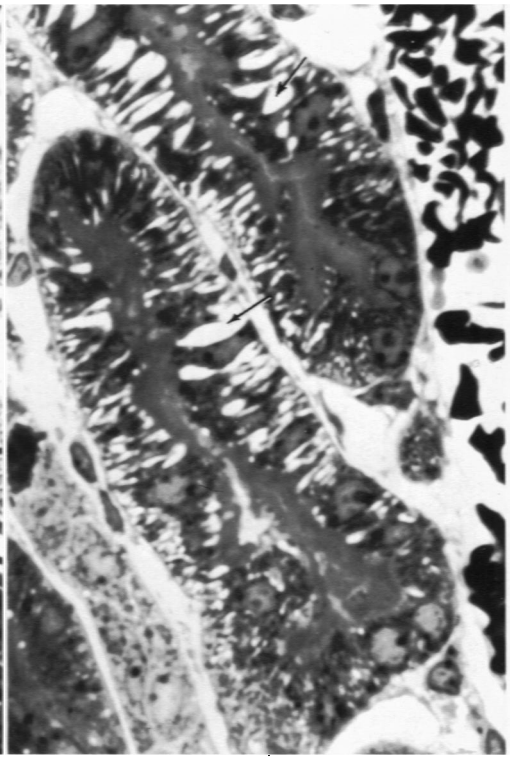

29

Fig 30. Electron micrograph of proximal tubule from renal biopsy fixed by immersion. Rearrangement of cellular organelles is striking, particularly near luminal surface. Microvilli forming brush border are greatly distorted. Elongate mitochondria are virtually nonexistent. System of apical vesicles, apical vacuoles, and apical dense tubules is barely recognizable. × 11,650.

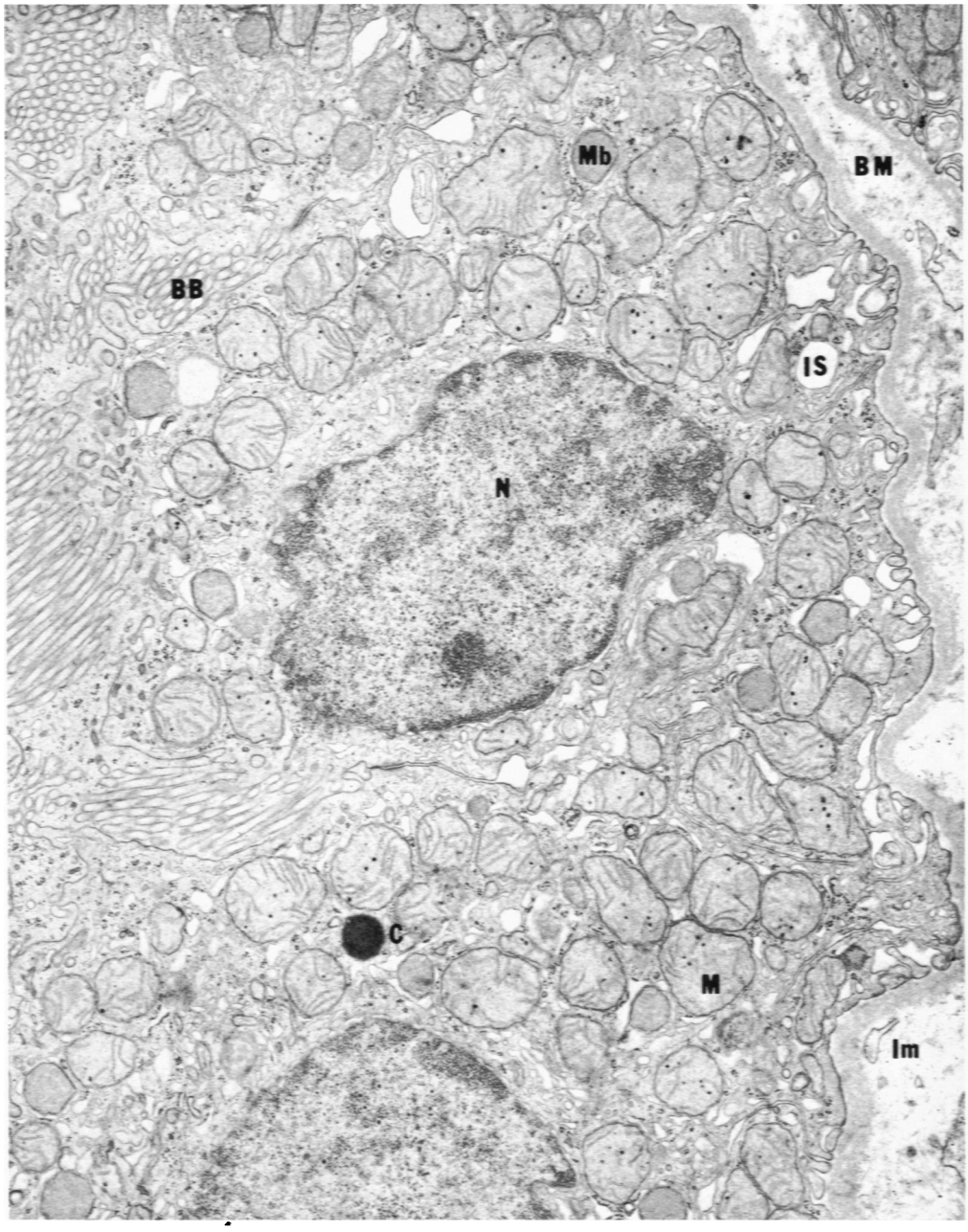

30

Fig 31. Electron micrograph showing mitochondrial inclusion lying entirely within widened cristae. Inclusions were composed of filaments 30–40 A in width which formed a helix 130–140 A in diameter with pitch of approximately 120 A. This was most common type of mitochondrial inclusion observed. × 47,400.

Fig 32. Electron micrograph showing second type of mitochondrial inclusion which was least common of the two and was always more electron dense than surrounding structures. It was composed of several parallel rows of membranes which resembled cristae. In some areas along these membranous profiles a periodicity of 290 A was present. This apparent periodicity appeared to be the result of twisting of parallel membranes to form double helix (*insert*). These structures were separated by 100 A space which was continuous with mitochondrial matrix. Short filaments with spacing of 90 A bridged this latter space at right angles to long membranous profiles. × 41,800. *Insert,* × 124,200.

Fig 33. Diagramatic representation of complex structure of second type of mitochondrial inclusion pictured in Fig 32. See text and Fig 32 legend for description.

Fig 34. Electron micrograph of two typical microbodies from biopsy tissue fixed by immersion. Their appearance is identical to microbodies from proximal tubules in areas of kidney not well preserved by IVIP. These organelles are swollen as evidenced by their increased volume, rarefaction of matrix, and bending of one or more marginal plates (*arrow*). Adjacent endoplasmic reticulum was widely dilated. × 35,700.

Fig 35. Electron micrograph of microbody from proximal tubule not well preserved by IVIP. Note that matrix is of approximately same density as that of mitochondrion at left. Both marginal plates have been fractured and bent (*arrows*), probaby as a result of swelling of organelle. × 79,500.

Fig 36. High power electron micrograph demonstrating fracture of microbody marginal plate with subsequent displacement of the two ends of plate (*arrow*). Matrix of microbody has same density as surrounding cytoplasm whereas, in optimally preserved microbodies fixed by IVIP, matrical density is greater than that of surrounding cytoplasm, regardless of fixative employed. × 96,950.

31

32

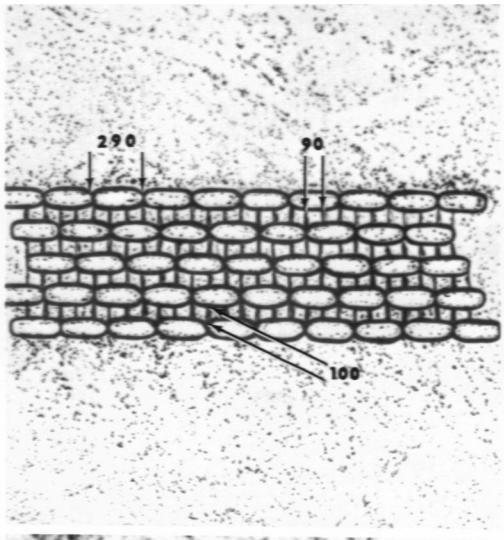

33

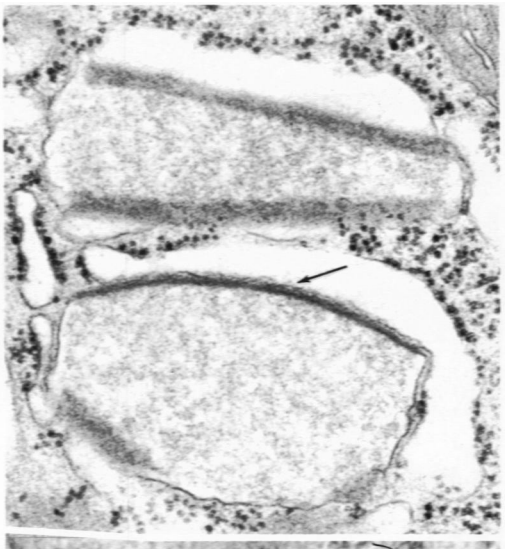

34

35

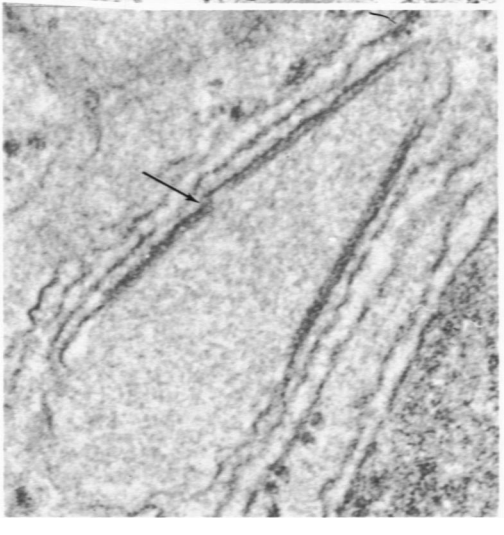

36

Fig 37. Electron micrograph showing pattern of positive staining (lead precipitate) indicating presence of acid phosphatase activity in typical cell of first segment of proximal tubule. Staining was limited to cytosomes and Golgi cisternae. Note widened intercellular spaces at right. × 10,450.

Fig 38. Electron micrograph of typical acid phosphatase reaction in proximal tubule cell characteristic of second segment. There was no discernible difference in pattern of reaction product in first and second segments of proximal tubule. Lead precipitate was confined to cytosomes and Golgi cisternae. × 11,800.

Fig 39. Higher power electron micrograph of two adjacent proximal tubule cells demonstrating specific localization of lead precipitate in Golgi cisternae at right. Pattern of precipitate in individual cytosomes varied considerably. × 15,150.

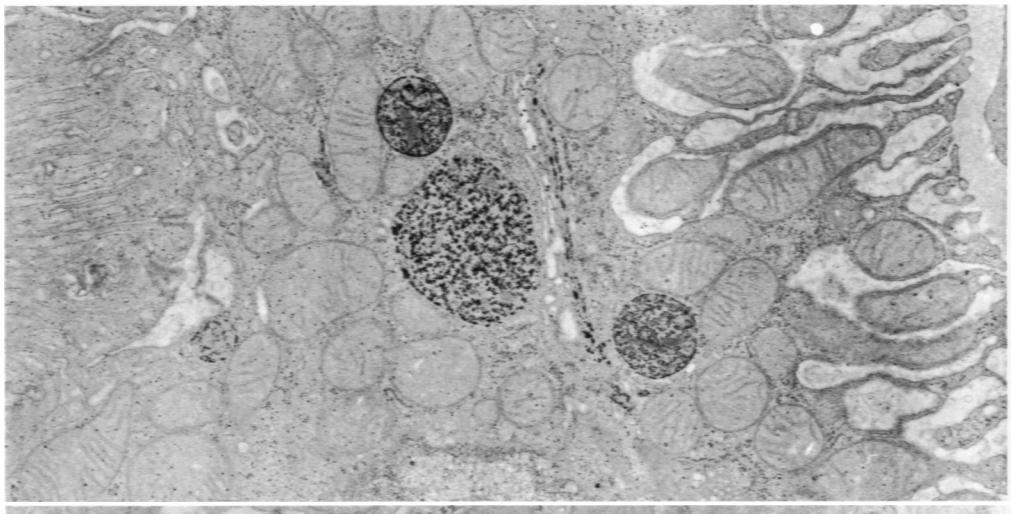

37

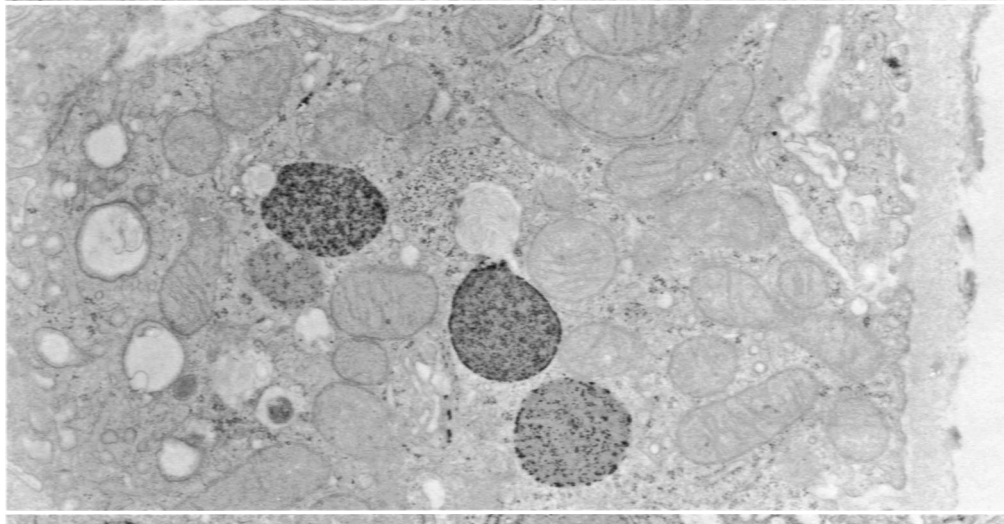

38

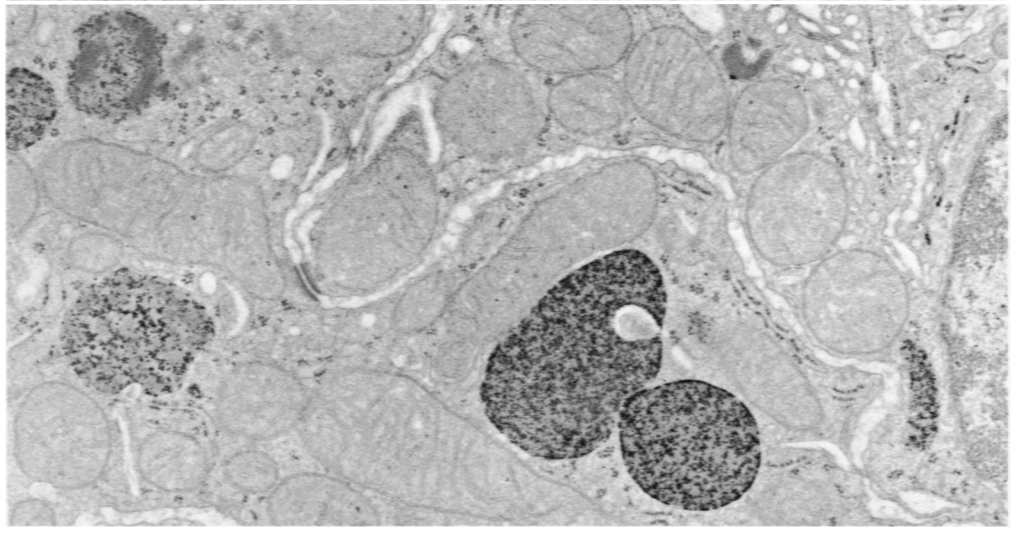

39